Journal of Translational Medicine

RESEARCH

Open Access

KLF14 directly downregulates the expression of GPX4 to exert antitumor effects by promoting ferroptosis in cervical cancer

Hui Ye[1,5], XuChao Ding[6], XinRan Lv[7], Ying Du[8], Rui Guo[9], Jin Qiu[2], RuoNan Li[2] and LiLi Cao[1,2,3,4*]

Abstract

Background Cervical cancer is the fourth leading cause of cancer-related death among women worldwide, and effective therapeutic strategies for its treatment are limited. Recent studies have indicated that ferroptosis, a form of regulated cell death, is a promising therapeutic strategy. KLF14 has been shown to regulate both cell proliferation and apoptosis in cervical cancer. However, its role in modulating lipid peroxidation and ferroptosis remains largely unexplored and enigmatic.

Methods SiHa and HeLa cells were transduced with lentiviral vectors to overexpress KLF14. Protein levels were analyzed via western blotting and immunohistochemistry (IHC). LDH assays, calcein-AM/propidium iodide (PI) staining, and generation of cell growth curves using a real-time cell analysis (RTCA) system were used to detect cell damage and proliferation. Cellular ROS, lipid ROS, transmission electron microscopy (TEM), and Fe^{2+} assays and a xenograft mouse model were used to measure the level of ferroptosis. Proteomics combined with bioinformatics methods was used to screen target genes regulated by KLF14, and CUT&Tag and dual-luciferase assays confirmed the repression of GPX4 by KLF14 via direct binding to its promoter.

Results KLF14 is abnormally expressed in various tumors and downregulated in cervical cancer. Overexpression of KLF14 induced ferroptosis and inhibited cell proliferation in vitro as well as xenograft tumorigenicity in vivo. Mechanistic studies revealed that KLF14 binds to the promoter of GPX4, suppressing its transcriptional activity and thereby decreasing its expression, which contributes to the induction of ferroptosis. Truncation and point mutation analyses of the GPX4 promoter revealed multiple binding sites for KLF14 within the − 1000 bp to + 35 bp region, which are responsible for its inhibitory effect on GPX4 transcription. Additionally, deletion of the zinc finger motif in KLF14 abolished its inhibitory effect on GPX4 promoter activity and cell proliferation.

Conclusion Our data revealed a previously unidentified function of KLF14 in promoting ferroptosis, which results in the suppression of cell proliferation. Mechanistically, we revealed a novel regulatory mechanism by which KLF14 targets GPX4. These findings suggest a novel strategy to induce ferroptosis through the targeting of KLF14 in human cervical cancer cells.

Keywords KLF14, GPX4, Ferroptosis, Promoter, Transcription factor, Cervical cancer

*Correspondence:
LiLi Cao
llcao@sdfmu.edu.cn

Full list of author information is available at the end of the article

Introduction

Cervical cancer is the fourth most prevalent type of cancer and the fourth leading cause of cancer-related death in women worldwide [1]. Although human papillomavirus (HPV) vaccination and screening strategies are effective at reducing mortality and morbidity, the mortality rate of cervical cancer remains relatively high, especially in low-income and middle-income countries [2]. Advanced or recurrent cervical cancer is generally incurable and has an extremely poor prognosis and a low survival rate [3]. Thus, it is necessary to explore the detailed molecular pathogenesis of cervical cancer to identify potential targets and new strategies for antitumor therapy.

Ferroptosis is a novel type of regulated cell death that is driven by excess accumulation of lipid peroxides in an iron-dependent manner [4, 5]. It is distinct from apoptosis, autophagic cell death and necroptosis. In recent years, numerous studies have revealed a tight link between ferroptosis and the progression and treatment of various cancers [6, 7], including cervical cancer [8–10], lung cancer [11] and clear cell renal cell carcinoma [12]. GPX4, a phospholipid hydroperoxide glutathione peroxidase, was the first-discovered central repressor of ferroptosis, and it contributes to tumor progression. GPX4 utilizes reduced glutathione (GSH) to reduce lipid hydroperoxides to lipid alcohols and protect the cell from ferroptosis [13]. Previous studies have shown that GPX4 is closely related to tumorigenesis, progression and malignant behaviors [14, 15]. Recent studies have reported the complex mechanisms of GPX4 in ferroptosis in cervical cancer. One study revealed that a deficiency in MTCH1 results in the downregulation of GPX4, ultimately inducing ferroptosis [9]. Another study revealed that circACAP2 interacts with miR-193a-5p, which targets GPX4, thereby repressing ferroptosis [16]. Additionally, PIN1 has been shown to influence ferroptosis through the NRF2/GPX4 axis, which confers sensitivity to cisplatin [17]. These findings demonstrated that ferroptosis has immense potential as a therapeutic target. Despite these advances, a comprehensive understanding of the regulatory mechanisms of ferroptosis in cervical cancer remains elusive and is not yet fully understood.

KLF14, a newly discovered member of the family, has zinc finger DNA-binding domains, similar to other members of the KLFs family. It has biological roles in multiple processes, including metabolism, immunity, and apoptosis [18]. In recent years, the role of KLF14 in tumors has been increasingly recognized, with evidence indicating that KLF14 regulates tumor cell proliferation, apoptosis, and metastasis [19]. Its inhibitory effects on various types of tumors have gained widespread attention. For example, survival analysis revealed that a low KLF14 level is associated with poor prognosis in human patients with colorectal cancer [20]. Another study reported that the long noncoding RNA (lncRNA) HAND2-AS1 inhibits colorectal cancer cell proliferation by promoting KLF14 expression [21]. KLF14 has also been reported to markedly suppress the growth and invasiveness of breast cancer cells [22, 23] and hepatocellular carcinoma cells [24, 25]. Our recent studies have shown that overexpression of KLF14 suppressed the expression of its target ITGB1 to induce apoptosis, thereby promoting cell death in cervical cancer [26]. In contrast, there are opposite reports on the function of KLF14 in different cancers. Luo et al. reported that KLF14 promoted cell growth by enhancing oxidative stress resistance in castrate-resistant prostate cancer [27]. Boot et al. reported that KLF14 was upregulated in thyroid cancer and that the knockdown of KLF14 reduced cell proliferation and initiated apoptosis [28]. These seemingly contradictory findings suggest that the function of KLF14 may be related to the type of tumor and its microenvironment. Despite extensive research on the role of KLF14 in tumor development, its involvement in ferroptosis has not been reported.

In this study, we discovered that overexpression of the transcription factor KLF14 triggered an increase in reactive oxygen species (ROS) accumulation and lipid peroxidation, which in turn promoted ferroptosis and suppressed cell proliferation in cervical cancer models, as observed both in vitro and in vivo. Interestingly, KLF14 was found to directly interact with the *GPX4* promoter, suppressing GPX4 expression and thereby modulating ferroptosis. Truncation of the zinc finger domain of KLF14 abolished the ability of KLF14 to inhibit GPX4 expression, thereby preventing it from suppressing cervical cancer cell proliferation. Given its pivotal role in controlling GPX4 expression and the progression of cervical cancer, KLF14 may be a promising therapeutic target. These findings could have significant implications for the development of novel anticancer therapies.

Methods

Cell lines and cell culture

Two human cervical cancer cell lines, SiHa and HeLa, were used in the present study. SiHa cells were purchased from the Chinese Tissue Culture Collection (CTCC; China). HeLa cells were obtained from the American Type Culture Collection (ATCC; USA). These cells were cultured in Dulbecco's modified Eagle medium (DMEM; Gibco, USA) supplemented with 10% fetal bovine serum (FBS; Gibco, USA) and 1% penicillin/streptomycin in a constant-temperature incubator at 37 °C with 5% CO_2.

Cell transfection

The human KLF14-overexpressing lentivirus and negative control lentivirus were synthesized by GeneChem (Shanghai, China). The human GPX4-overexpressing

lentivirus and negative control lentivirus were synthesized by Beijing Syngenbio Co., Ltd. (Beijing, China). The KLF14 truncation mutant lentivirus and negative control lentivirus were provided by Beijing Syngenbio Co., Ltd. (Beijing, China). Lentiviral transduction and the generation and preculture of stable cell lines were performed as previously described [26].

Immunohistochemistry (IHC)

A human cervical cancer tissue microarray (OD-CT-RpUtr-03-005) containing 31 cervical cancer tissues and paired adjacent tissues was purchased from Shanghai Xinchao Biotechnology Co., Ltd. The mean age of the patients was 43.7 years. The participants in this study were diagnosed with primary cervical cancer, all of which were squamous cell carcinomas. Most of the cases were pathologically graded as G2, and the clinical stage was stage II. All participants provided informed consent to participate in the study, in accordance with relevant ethical standards. The procedure for IHC analysis was conducted as described in our previous study [26]. Mouse tumor tissue samples were fixed with 4% paraformaldehyde, embedded in paraffin, and cut into 4 μm thick sections for hematoxylin/eosin (HE) staining and IHC staining. For the IHC analysis, antibodies against KLF14, GPX4 and 4-hydroxynonenal (4-HNE) were used. HE and IHC staining were performed using Leica ST5020 (Leica Biosystems) and Dako Autostainer Link 48 (Dako, USA) slide stainers, respectively. The antibodies used in this study were specific for KLF14 (Sigma, # HPA044729, 1:2000), GPX4 (Abcam, # ab125066, 1:5000) and 4-HNE (Abcam, #ab48506, 1:500).

Animal model

Female 4–5-week-old BALB/c nude mice were purchased from the Vital River Laboratory Animal Technology (Beijing, China). To reduce potential variability inherent to individual nude mice, equal quantities of SiHa/KLF14 control cells and SiHa/KLF14-overexpressing cells were matched and respectively injected into symmetrical subcutaneous sites of a single nude mouse. All the mice were monitored for general health and tumor growth throughout the experiment. Tumor volume was determined using the formula V = (longest diameter) × (shortest diameter)^2/2. A growth curve for tumor volume was then plotted. After approximately 38 days, the nude mice were humanely euthanized while under anesthesia. Xenograft tumors were harvested, and tumor tissues were processed for protein extraction and IHC analysis. The Ethics Committee of the First Affiliated Hospital of Shandong First Medical University approved this study (SYDWLS2020016). The animal experiments were conducted in strict accordance with national legislation, rules, and standards pertaining to the use of experimental animals, including adherence to the Regulations on the Management of Experimental Animals and the Guidelines for Ethical Review of Experimental Animal Welfare. Additionally, the studies were guided by the widely accepted standards for reporting animal research as outlined in international biomedical publications, specifically the Animal Research: Reporting of In Vivo Experiments (ARRIVE) Guidelines.

Western blotting

Cell lysates were prepared in radioimmunoprecipitation assay (RIPA) buffer containing a proteinase inhibitor. Proteins in the samples were separated by SDS-PAGE and then electroblotted onto PVDF membranes (Millipore, USA). The membranes were then blocked in TBST containing 5% nonfat milk for one hour, washed with TBST 3 times (5 min each), and then incubated overnight with a primary antibody at 4 °C. After being washed with TBST 3 times (10 min each), the membranes were incubated with the corresponding secondary antibody diluted with blocking buffer at room temperature for 1 h. The membranes were then washed three more times with TBST (10 min each), and signals were visualized by enhanced chemiluminescence (ECL) using Immobilon ECL Ultra Western HRP Substrate (Millipore). The experiment was independently replicated three times.

Primary antibodies against FLAG (CST, #14793S, 1:1000), KLF14 (Invitrogen, #PA5-23784, 1:1000), GPX4 (CST, #52455S, 1:1000), GAPDH (CST, #5174S, 1:1000), and β-actin (Boster, # BM0627, 1:1000) and secondary antibodies against rabbit IgG (CST, #7074, 1:10000) and mouse IgG (CST, #7076, 1:10000) were used.

Cell counting kit-8 (CCK-8) assay

Cells from both the control and KLF14-overexpressing groups were cultured in 96-well plates alongside a blank well containing medium only. Once the cells had fully adhered to the well surface (after 3 to 6 h), the optical density (OD) at 450 nm was measured to establish the baseline cellular state at time zero (0 days). The medium was subsequently replaced with doxycycline (DOX)-supplemented medium for incubation. On days 1, 2, 3, 4 and 5, the CCK-8 reagent (#CK04, Dojindo) was added to the wells to evaluate cell proliferation. The assays were performed three times in triplicate.

Cytotoxicity LDH release assay

The release of LDH from cervical cancer cells was assessed using the LDH assay kit (Dojindo, CK12). SiHa cells, at a density of 8×10^3 per well, were seeded into a 96-well microplate and cultured for 48 h in medium supplemented with DOX. According to the manufacturer's protocol, 100 μl of working solution was added to each well. After 30 min of incubation, stop solution was added,

followed by detection using a microplate reader (BioTeck, Synergy H1) at 490 nm, and the % of LDH released was then calculated applying the formula: 100 × (experimental LDH release-culture medium background)/(maximum LDH release- culture medium background). The experiment was performed three independent times.

Calcein-AM/propidium iodide (PI) staining

A Calcein-AM/PI cell viability/cytotoxicity assay kit (Cat. No. C2015S) were purchased from Beyotime. Cells from both the control and KLF14-overexpressing groups were cultured in 35-mm confocal dishes (NEST). After a 24-hours of exposure to DOX, the cells were stained with calcein-AM /PI (each concentration was diluted 1000-fold) and incubated at 37 °C in the dark for 30 min. Subsequently, fluorescence imaging was captured using a confocal microscope (Zeiss Cell Discoverer 7). The experiment was performed three independent times.

Proteome sequencing

KLF14-overexpressing SiHa cells and control SiHa cells were separately seeded into 10 cm dishes, DOX was added to induce the overexpression of KLF14 and the cells were cultured for an additional 24 h. Most of the culture medium was discarded from the dish, leaving a thin layer of medium that covered the bottom of the dish. The cells were collected using a cell scraper and centrifuged at *500* × *g* for 5 min, after which the supernatant was discarded. KLF14-overexpressing SiHa cells and control SiHa cells were harvested, and three biological replicates per condition were established. Tandem mass tag (TMT)-based quantitative proteomics and subsequent bioinformatics analysis of the sequencing data were conducted by Shanghai Zhongke New Life Biotechnology Co., Ltd.

Flow cytometry

Intracellular ROS and lipid ROS were quantified using the DCFH-DA fluorescent dye (Beyotime, S0033S) and the C11-BODIPY 581/591 fluorescent probe (Invitrogen, D3861), respectively. DCFH-DA and BODIPY-C11 were added to the cells at a concentration of 10 μM. Following a 30-minute incubation at 37 °C, the cells were washed with PBS, trypsinized to obtain a single-cell suspension, and subsequently analyzed with an ACEA NovoCyte Flow Cytometer (Agilent Technologies, Santa Clara). The experiment was performed three independent times.

Measurement of the intracellular Fe^{2+} concentration

The intracellular Fe^{2+} concentration was quantified using a FerroOrange assay kit (Dojindo, F374), following the provided protocol. Cells were seeded into 35-mm confocal dishes. After 48 h of culture in medium supplemented DOX, the cells were treated with FerroOrange dye at 1 μmol/L and incubated at 37 °C for 30 min. Fluorescence images were acquired with a confocal laser scanning microscope. The experiment was performed three independent times.

Transmission electron microscopy

The cells and tissues were fixed with cold electron microscopy fixative (Servicebio, G1102) for 2–3 h at room temperature. The samples were subsequently washed three times with PBS, fixed with 1% osmium tetroxide for 1.5 h, and dehydrated in ethanol and acetone. The samples were then embedded, sectioned, and stained with uranyl acetate and lead citrate. Images were acquired using a Hitachi HT-7800 transmission electron microscope (80 kV).

Evaluation of proliferation by real-time cell analysis (RTCA)

RTCA was performed to assess cell proliferation using the xCELLigence system (Agilent). Initially, 50 μL of culture medium was added to each well of an E-plate 16. The E-plate was then connected to the device for baseline impedance recording. After a confirmatory reading, 100 μL of a cell suspension was added, and the plate was incubated at room temperature for 30 min to facilitate cell adhesion. Subsequently, the E-plate was returned to the xCELLigence system within the incubator for continuous monitoring of cell growth. This study was performed in triplicate, with each trial including two replicate wells.

Dual-luciferase reporter assay

The KLF14 plasmid was constructed by GeneChem (Shanghai, China). The *GPX4* wild-type (*GPX4-WT*) promoter plasmid and various truncation plasmids were constructed by Beijing Syngenbio Co., Ltd. (Beijing, China). The *GPX4* promoter point mutation plasmid was constructed by Hanyin Biotechnology (Shanghai, China).

HEK-293T cells were cultured in 24-well plates and transfected with varying concentrations of expression plasmids and a Renilla luciferase control plasmid using PolyJet Transfection Reagent (SignaGen). Forty-eight hours post transfection, firefly and renilla luciferase activities were measured with a dual luciferase assay (Promega) following the manufacturer's protocol, and the relative luciferase activity was quantified. The experiment was performed three independent times.

CUT&tag experiment and data analysis

SiHa cells were prepared as a suspension, and their viability was assessed using trypan blue staining. The cells were then processed in accordance with the standard operating procedure provided with the HyperactiveR Universal CUT&Tag Assay Kit for Illumina (Vazyme Biotech, TD903, Nanjing, China) to isolate DNA fragments bound to the KLF14 transcription factor. DNA library

construction and amplification were subsequently performed using the TruePrepR Index Kit V2 for Illumina (Vazyme, TD202). The qualified DNA libraries were subsequently submitted to Novogene (Novogene, Beijing, China) for sequencing and data analysis.

The sequencing data were processed using Fastp software to trim the raw reads and obtain clean reads. Subsequently, the computeMatrix function in deepTools software was used to quantify CUT&Tag signals within a 3 kb region surrounding each transcription start site (TSS). To pinpoint conserved sequence features at peak enrichment locations, hypergeometric optimization of motif enrichment (HOMER) software was applied to analyze sequences spanning a region 250 bp upstream and downstream of the peak summit, covering a total of 500 bp. ChIPseeker software was then utilized to evaluate the distribution of these peaks across diverse functional genomic regions. Differential binding analysis was conducted based on the Fold Enrich values of the peaks from distinct experimental groups. Peaks exhibiting a Fold Enrich ratio of more than 2 were designated differentially bound peaks, highlighting the variable binding sites across the experiments. These differential binding sites were mapped to their corresponding genes, which were subsequently subjected to GO and Kyoto Encyclopedia of Genes and Genomes (KEGG) analyses to elucidate their biological significance. The alignment was then visualized using Integrative Genomics Viewer (IGV) software (version 2.16.0).

Immunofluorescence assay

An immunofluorescence assay was used to detect the protein of KLF14 and its zinc-finger structural mutants in SiHa cells. Cells were seeded into 35-mm confocal dishes. The cells were cultured for 48 h in medium containing DOX. The cells were fixed with 4% paraformaldehyde for 10 min and then permeabilized with 0.1% Triton X-100 for 10 min. After the samples were blocked with 5% BSA for 30 min at 37 °C, they were incubated with a primary antibody against Flag (CST, #14793S, 1:500) overnight at 4 °C. The cells were subsequently incubated with an Alexa Fluor® 647 secondary antibody (Abcam, #ab150083, 1:500) for 60 min, followed by DAPI (Beyotime, #C1006) staining for 10 min at room temperature. Images were captured using a confocal microscope (Zeiss Cell Discoverer 7).

Drugs and other reagents

Liproxstatin-1 (lip-1) (SJ-MX0055) was purchased from SparkJade. RSL3 (HY-100218 A) and DOX (HY-N0565) were purchase from MCE.

Bioinformatics analysis

We analyzed the expression of KLF14 in normal and tumor tissues using the UALCAN database (http://ualcan.path.uab.edu/) [29]. We performed a Kaplan-Meier survival analysis using the KM plotter online database (http://kmplot.com) [30]. We identified genes associated with ferroptosis using the Gene Cards (https://www.genecards.org/) and FerrDb (http://www.zhounan.org/ferrdb) databases. A Venn diagram was generated to display the genes shared between the ferroptosis-related gene sets and those identified via proteome sequencing of the DEPs. Further analysis of these genes, including KEGG and GO enrichment analyses, was conducted via Metascape (http://metascape.org). The Search Tool for the Retrieval of Interacting Genes/Proteins (STRING) database was used to construct a protein–protein interaction (PPI) network of the DEPs related to ferroptosis. The results were then imported into Cytoscape (version 3.9.1) for further analysis using the CytoHubba plugin to identify key hub genes. Heatmaps were constructed for visualization using the heatmap package.

Statistical analysis

Data analysis was performed with GraphPad Prism 8.0. All the statistical analyses were based on at least three independent measurements. Unpaired Student's t test, one-way ANOVA and two-way ANOVA were used to analyze the data. A p value less than 0.05 was considered to indicate statistical significance.

Results

Expression and prognostic analysis of *KLF14* in pan cancer

To investigate the expression patterns of *KLF14* in various human cancers, we performed a pan cancer analysis using publicly available datasets from The Cancer Genome Atlas (TCGA) obtained via the UALCAN database (Fig. 1A). *KLF14* is abnormally expressed in many cancers. Specifically, compared with that in normal tissues, *KLF14* was notably downregulated in breast invasive carcinoma (BRCA), kidney chromophobe (KICH), kidney renal papillary cell carcinoma (KIRP), lung squamous cell carcinoma (LUSC), pheochromocytoma and paraganglioma (PCPG), stomach adenocarcinoma (STAD), uterine corpus endometrial carcinoma (UCEC), and it was notably upregulated in esophageal carcinoma (ESCA), bladder urothelial carcinoma (BLCA) and cholangiocarcinoma (CHOL), head and neck squamous cell carcinoma (HNSC). Next, we conducted a Kaplan-Meier survival analysis via online tool (http://kmplot.com/analysis/) and found that the level of KLF14 expression was correlated with overall survival (OS) and relapse-free survival (RFS) (Fig. 1B-J). Interestingly, the K-M curve revealed that elevated KLF14 expression was correlated with prolonged OS in liver hepatocellular carcinoma

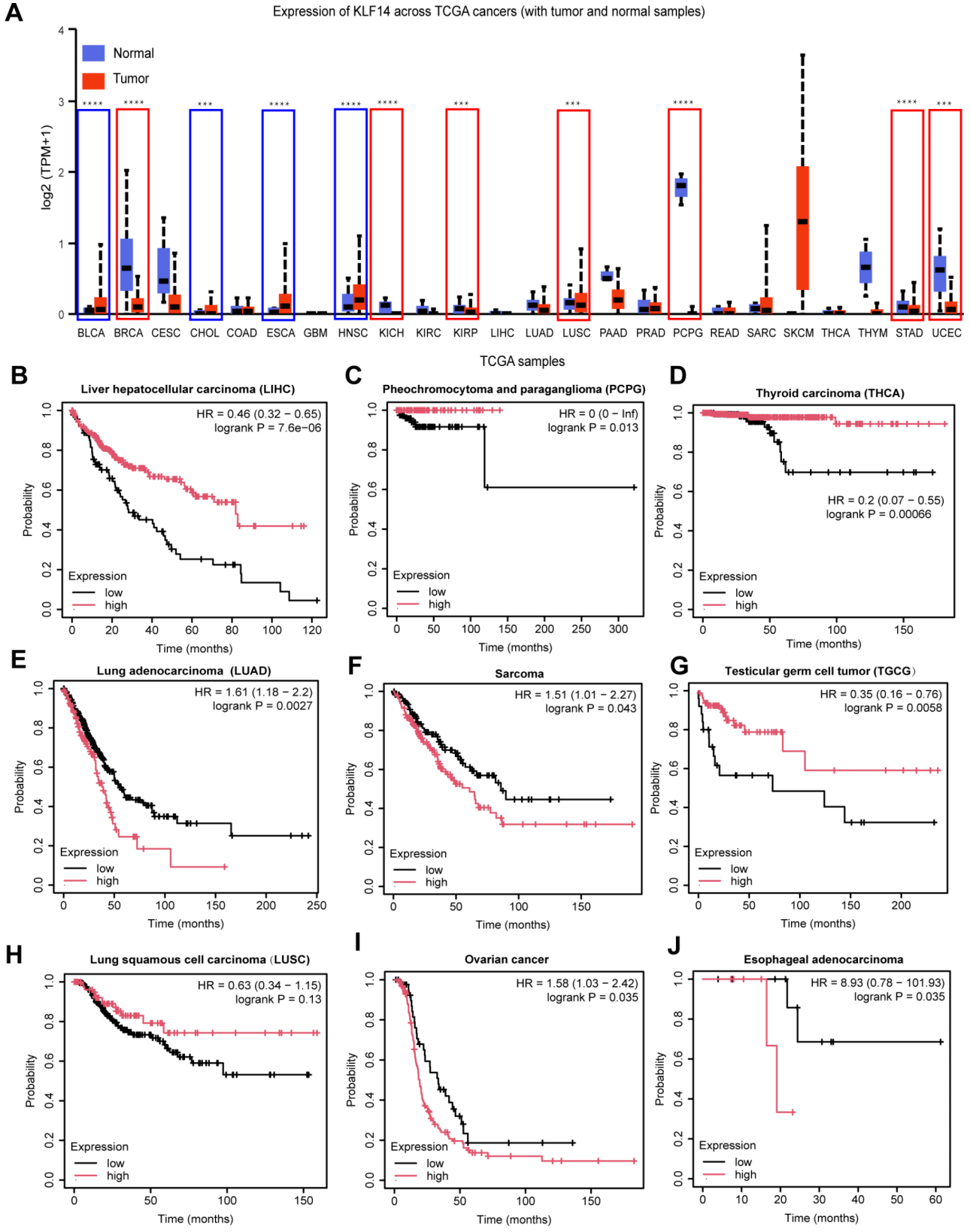

Fig. 1 The expression and prognostic analysis of KLF14 in pan cancer. (**A**) The expression of KLF14 mRNA in tumor and normal tissues was analyzed using TCGA data obtained via UALCAN (A, the red box indicates that the expression of KLF14 in tumor tissue is significantly lower than in normal tissue, the blue box indicates that the expression of KLF14 in tumor tissue is significantly higher than that in normal tissue). (**B**-**J**) Overall survival (OS) (**B**-**F**) and relapse-free survival (RFS) (**G**-**J**) curves of cancers with different KLF14 expression levels in Kaplan-Meier plotter database. ***$p < 0.001$. ****$p < 0.0001$

(LIHC), PCPG and thyroid carcinoma (THCA), but decreased OS in lung adenocarcinoma (LUAD) and sarcoma (Fig. 1B-F). Subsequent analyses for RFS indicated that upregulated KLF14 was significantly associated with better RFS in testicular germ cell tumor (TGCT), but poor RFS in ovarian cancer and esophageal adenocarcinoma (Fig. 1G-J). The data revealed that KLF14 expression was linked to variable prognostic results among different cancers. Ultimately, the findings indicate that KLF14 could serve as a prognostic biomarker for various cancer types. However, the variable associations observed among cancer types highlight the complexity of its role and the need for further investigation to understand these differences. Our subsequent research explored the significance of KLF14 expression in cervical cancer.

KLF14 is downregulated in cervical cancer and accelerates cell death in cervical cancer cells

By searching the Human Protein Atlas (HPA) database, we found that KLF14 was significantly downregulated in cervical cancer tissues compared with normal cervical tissues (Fig. 2A). Our analysis of tissue microarray data revealed that KLF14 was also significantly downregulated in cervical cancer tissue compared with adjacent noncancerous tissue (Fig. 1S A-B). These results indicate that KLF14 may act as a suppressor of tumorigenesis in cervical cancer. We next established SiHa and HeLa cell lines with stable overexpression of KLF14 in SiHa and HeLa cells via lentiviral transduction, and KLF14 overexpression was confirmed by western blotting, as shown in Fig. 1S C-E. To assess the effect of KLF14 on cervical cancer cells, we conducted a LDH release assay and discovered that overexpression of KLF14 markedly promoted the LDH release in SiHa cells (Fig. 2B). Additionally, we assessed the effect of KLF14 on cell viability using Calcein AM/PI staining. The results revealed that overexpression of KLF14 significantly promoted cell death in SiHa and HeLa cells against control group (Fig. 2C). Taken together, these findings suggest that KLF14 is expressed at low levels in cervical cancer cells, potentially acting as a pivotal tumor suppressor by promoting cell death mechanisms.

Proteomic analysis identified differentially expressed proteins (DEPs) in cervical cancer cells after KLF14 overexpression

Our previous study revealed that KLF14 overexpression inhibited the proliferation and facilitated the apoptosis of cervical carcinoma cells [26]. However, the detailed molecular regulatory mechanism remains to be determined. Thus, we overexpressed KLF14 in SiHa cells and performed TMT-based quantitative proteomic analysis of three independent replicates. To investigate whether other types of antitumor mechanisms could be involved, we performed bioinformatics analysis. A total of 3257 (1645 upregulated and 1612 downregulated) DEPs were identified between the KLF14-overexpressing group (OE-KLF14) and the control group (OE-NC) (Fig. 3A, Fig. 2S A). Next, the DEPs were subjected to Gene Ontology (GO) functional annotation analysis, which revealed that they were strongly related to the GO terms biological regulation, regulation of biological process and metabolic process (Fig. 2S B), as well as iron ion binding and protein kinase binding (Fig. 2S C). These findings suggest that DEPs have the potential to be involved in diverse cellular pathways for functional regulation. KEGG pathway annotation of all the DEPs showed that pathways related to the cell cycle, apoptosis, and cancer were strongly correlated with the DEPs (Fig. 2S D). To explore potential interactions among the DEPs, we constructed a protein–protein interaction (PPI) network (Fig. 2S E). Our analysis revealed that most of the proteins selected for analysis had mutual direct or indirect interactions. These findings suggest that KLF14 may influence gene transcription and cellular functions such as proliferation, apoptosis, and metabolism by interacting with multiple molecules and pathways.

KLF14 induces ferroptosis in cervical cancer cells

Ferroptosis is a type of iron dependent, nonapoptotic cell death characterized by iron overload, elevated ROS levels and lipid peroxidation. We identified several important ferroptosis-related proteins among the 3257 DEPs. To gain a more comprehensive understanding, we downloaded 484 and 635 ferroptosis-associated genes from FerrDb and the GeneCards database, respectively. An online Venn diagram tool was used to identify the overlapping DEGs, which comprised 66 genes, 28 of which were upregulated and 38 of which were downregulated (Fig. 3B-C; Table 1S). To identify the functions and pathways related to the associated DEPs, enrichment analysis was performed via the Metascape online tool. GO enrichment analysis revealed enrichment of some of the DEPs in the terms response to oxidative stress (GO:0006979), oxidoreductase activity (GO:0016491), monocarboxylic acid metabolic process (GO:0032787), regulation of lipid biosynthetic process (GO:0046890), regulation of generation of precursor metabolites and energy (GO:0043467) and cellular transition metal ion homeostasis (GO:0046916) (Fig. 3D). KEGG pathway enrichment analysis indicated that the ferroptosis pathway (hsa04216) was significantly enriched in the DEPs (Fig. 3E).

To explore whether KLF14 triggers ferroptosis, we added the ferroptosis inhibitor lip-1 to SiHa cells and generated a cell proliferation curve with an RTCA system. Lip-1 partly reversed the KLF14-mediated

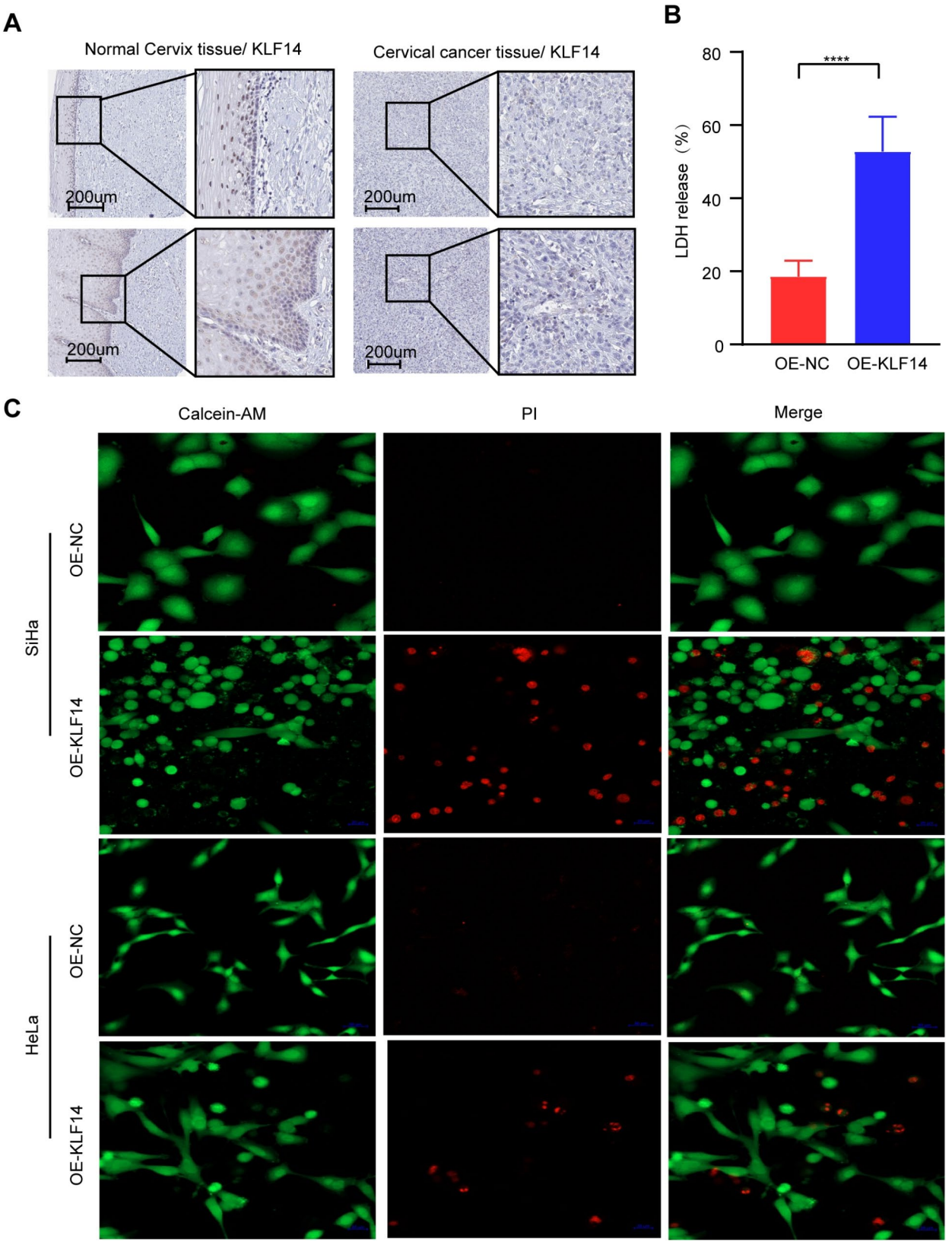

Fig. 2 KLF14 is downregulated in cervical cancer and accelerates cell death in cervical cancer cells. (**A**) Representative IHC images indicating KLF14 expression retrieved from the HPA database. (**B**) The LDH release rate of SiHa cells. The data are presented as the means ± SDs. $N = 3$ independent repeats. p values were calculated via an unpaired t test. (**C**) Calcein AM/PI staining of SiHa and HeLa cells. The green signal indicates live cells, whereas the red signal indicates dead cells. The experiment was independently repeated three times, each yielding similar results. ****$p < 0.0001$

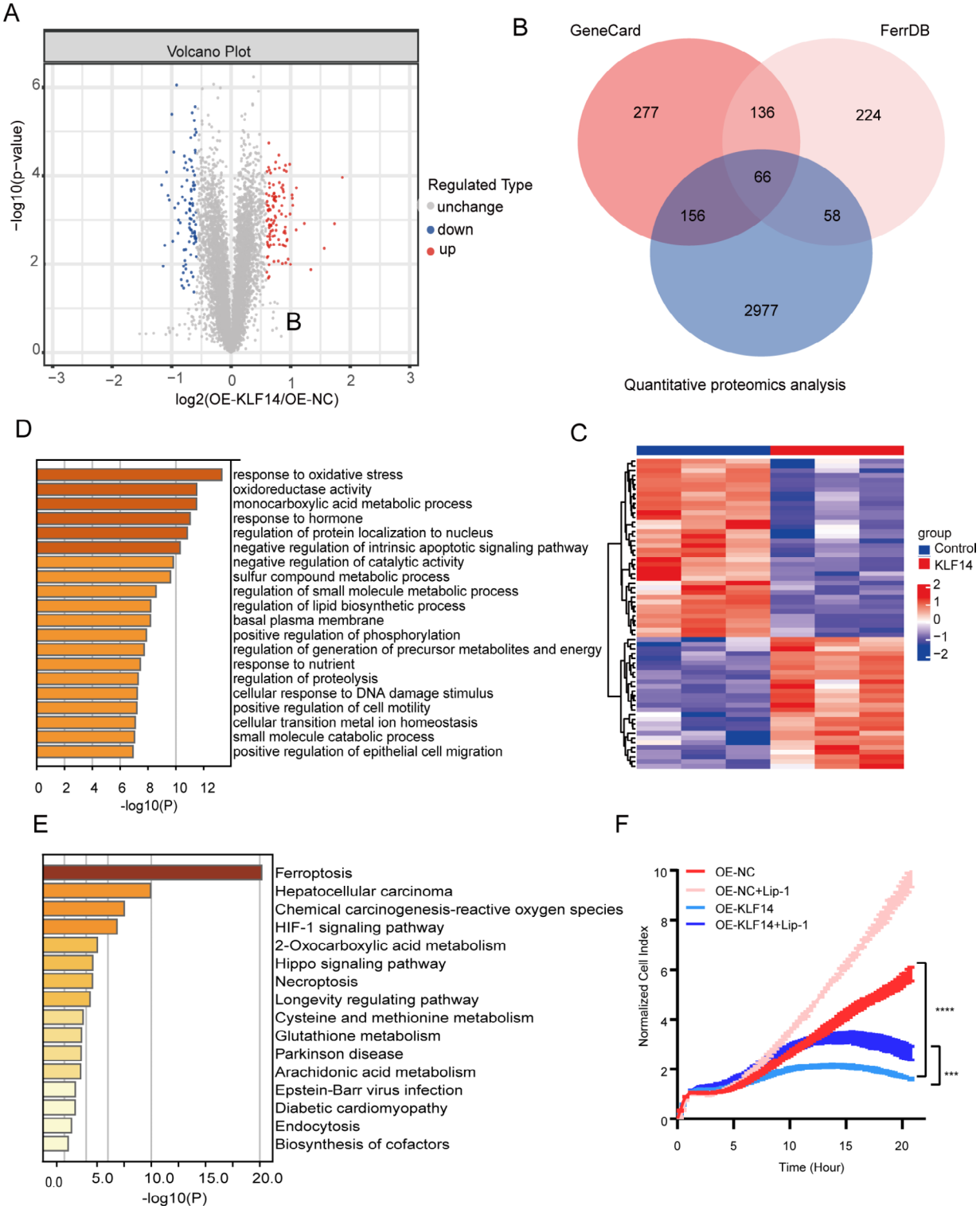

Fig. 3 KLF14-overexpressing SiHa cells DEPs are involved in ferroptosis-related biological processes and pathways. (**A**) Volcano plot showing differentially expressed proteins (DEPs) via TMT-based quantitative proteomics. (**B**) Venn diagram showing the overlap between the DEGs and ferroptosis-related genes. (**C**) Heatmap of the 66 ferroptosis-related DEGs. (**D**) GO enrichment analysis of the 66 ferroptosis-related DEGs. (**E**) KEGG pathway enrichment analysis of the 66 ferroptosis-related DEGs. (**F**) Real-time cell analysis (RTCA) of SiHa cell proliferation with the xCELLigence system. Each experiment was performed with 2 technical repeats and was independently repeated three times. p values were calculated via the Kruskal-Wallis test. ***$p < 0.001$, ****$p < 0.0001$

inhibition of SiHa cell proliferation (Fig. 3F). We also measured the levels of intracellular ROS and lipid ROS by flow cytometry using the ROS detection dye 2',7'-dichlorodihydrofluorescein diacetate (DCFH-DA) and the lipid ROS probe C11 BODIPY 581/591, respectively. Notably, after KLF14 overexpression, both the ROS and lipid ROS levels were significantly higher than those in the control group (Fig. 4A-D). Moreover, the ability of KLF14 overexpression to promote ROS and lipid ROS is comparable to or even stronger than that of RSL3 in SiHa and HeLa cells. Additionally, the additive or synergistic effect of KLF14 with RSL3 was greater than that of KLF14 overexpression alone. Next, we estimated the intracellular level of Fe^{2+} using the specific fluorescent probe FerroOrange via confocal microscopy and found that the signal intensity of FerroOrange was markedly increased in KLF14-overexpressing SiHa cells, and similar to that in the control group with added RSL3 (Fig. 4E). Mitochondrial shrinkage and disruption of mitochondrial cristae are typical features of ferroptosis. We thus examined these characteristics by TEM. As expected, the TEM images revealed morphological alterations typical of ferroptosis in the KLF14-overexpressing SiHa cells compared with the control cells. The mitochondria became smaller, and the number of mitochondrial cristae was reduced in number or even absent (Fig. 4F). Taken together, these data suggest that KLF14 indeed triggers ferroptotic death in cervical cancer cells.

KLF14 induces ferroptosis and inhibits cell proliferation by downregulating GPX4

To further explore the molecular mechanism related to the KLF14-mediated ferroptosis phenotype in cervical cancer cells, we performed a PPI network analysis on the 66 ferroptosis-related DEGs using the STRING and Cytoscape (Fig. 5A). The top ten hub genes were identified from the PPI network (Fig. 5B), and their expression patterns were visualized via a heatmap (Fig. 5C). Among the hub genes, GPX4 is not only a marker of ferroptotic cell death but also an essential regulator [13]. It utilizes reduced GSH to reduce the accumulation of lipid peroxides to protect cells from ferroptosis. The clustering heatmap of the ten hub genes related to ferroptosis revealed that after overexpression of KLF14, the expression of GPX4 significantly changed (Fig. 5C). We therefore focused our further analysis on the *GPX4* gene. To support our findings, we evaluated whether KLF14 regulates GPX4 protein expression. The protein expression level of GPX4 in both SiHa and HeLa cells was markedly decreased after KLF14 overexpression compared with that in the corresponding control cells (Fig. 5D-F). To evaluate whether the ferroptosis-promoting effect of KLF14 is dependent on the downregulation of GPX4, we performed rescue experiments. We generated a GPX4-overexpressing lentivirus and the corresponding control lentivirus. These lentiviruses were used to infect SiHa cells in the stable KLF14 overexpression and control groups. The overexpression efficiency was then verified by Western blot analysis (Fig. 5G-H). Transduction of the KLF14 overexpression construct alone significantly increased ROS and lipid ROS production, and these effects were partially reversed by cotransfection with the GPX4 overexpression construct (Fig. 5I-L). The results of the RTCA (Fig. 5M) and CCK-8 assays (Fig. 5N) revealed that GPX4 overexpression partly reversed the suppressive effects of KLF14 overexpression on SiHa cells. These results show that KLF14 regulates ferroptosis and inhibits cell proliferation partially by modulating the expression of GPX4 in cervical cancer.

KLF14 acts as a transcriptional repressor of GPX4 by directly binding to its promoter

To explore the molecular mechanism of KLF14-mediated ferroptosis and identify the direct transcriptional targets of KLF14, we performed CUT&Tag-seq for KLF14 to map the genome-wide binding of KLF14 in SiHa cells overexpressing KLF14. CUT&Tag-seq analysis revealed that a significant proportion of the identified KLF14 binding peaks were localized around TSSs (Fig. 6A). As shown in Fig. 6B, KLF14 binding sites were identified in both promoter and nonpromoter regions, with approximately 53.5% of the KLF14-bound sites located within a 1-kb region upstream of the TSS. A total of 19048 genes with KLF14 binding sites were annotated. As expected, the most enriched known motifs matched the KLF14-binding motifs (Fig. 6C). Known motif enrichment analysis and de novo motif analysis via HOMER revealed that the KLF14, AZF1, SCL, STZ, KLF5, Maz, ZNF711, RAP211, KLF6, TF3A, MUB and Elk4 genes harbored the most significantly enriched DNA-binding motifs within KLF14-bound regions, suggesting their potential role as functional mediators of KLF14 activity (Fig. 6C-D). Among the KLF14 peaks, 36,153 were found in the KLF14-overexpressing group but not in the control group, as shown in Fig. 6E. In addition, GO enrichment analysis of the genes associated with the differential peaks revealed associations with the terms regulation of binding, protein binding, cellular metabolic process, positive regulation of cellular metabolic process and cell differentiation (Fig. 6F). Moreover, KEGG pathway analysis showed the possible associations of the target genes with pathways related to Parkinson's disease, the mTOR signaling pathway, the HIF-1 signaling pathway, apoptosis, Alzheimer's disease, oxidative phosphorylation, and the wnt signaling cascade (Fig. 6G). Subsequently, we examined the overlap between the CUT&Tag-seq and proteomics datasets, revealing 1531 targets whose expression was directly controlled by KLF14 deficiency

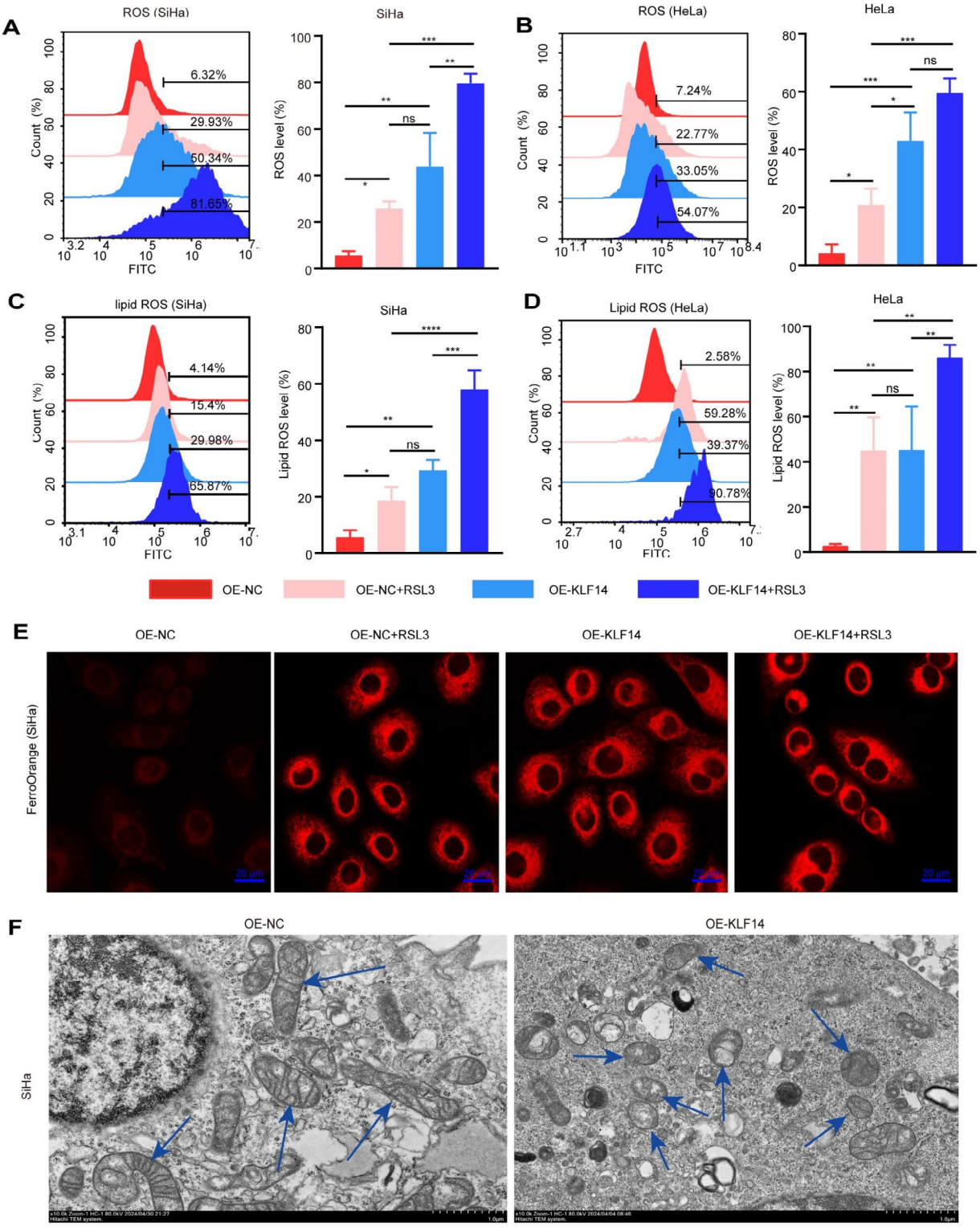

Fig. 4 KLF14 induces ferroptosis in cervical cancer cells. (**A**-**B**) The intracellular ROS levels in SiHa and HeLa cells were quantified via flow cytometry using DCFH-DA staining. The data are presented as the means ± SDs. $N = 3$ independent repeats. p values were calculated using one-way ANOVA test. (**C**-**D**) The accumulation of lipid ROS in SiHa and HeLa cells was evaluated via flow cytometry using the BODIPY C11 probe. The data are presented as the means ± SDs. $N = 3$ independent repeats. p values were calculated using one-way ANOVA test. (**E**) Representative images of intracellular Fe^{2+} acquired by laser confocal microscopy using the fluorescent probe FerroOrange. The experiment was independently repeated three times, each yielding similar results. (**F**) TEM images of the ultrastructures of control and KLF14-overexpressing SiHa cells (blue arrows represent mitochondria). The experiment was independently repeated two times with similar results. ns: not statistical significant. *$p < 0.05$, **$p < 0.01$, ***$p < 0.001$, ****$p < 0.0001$

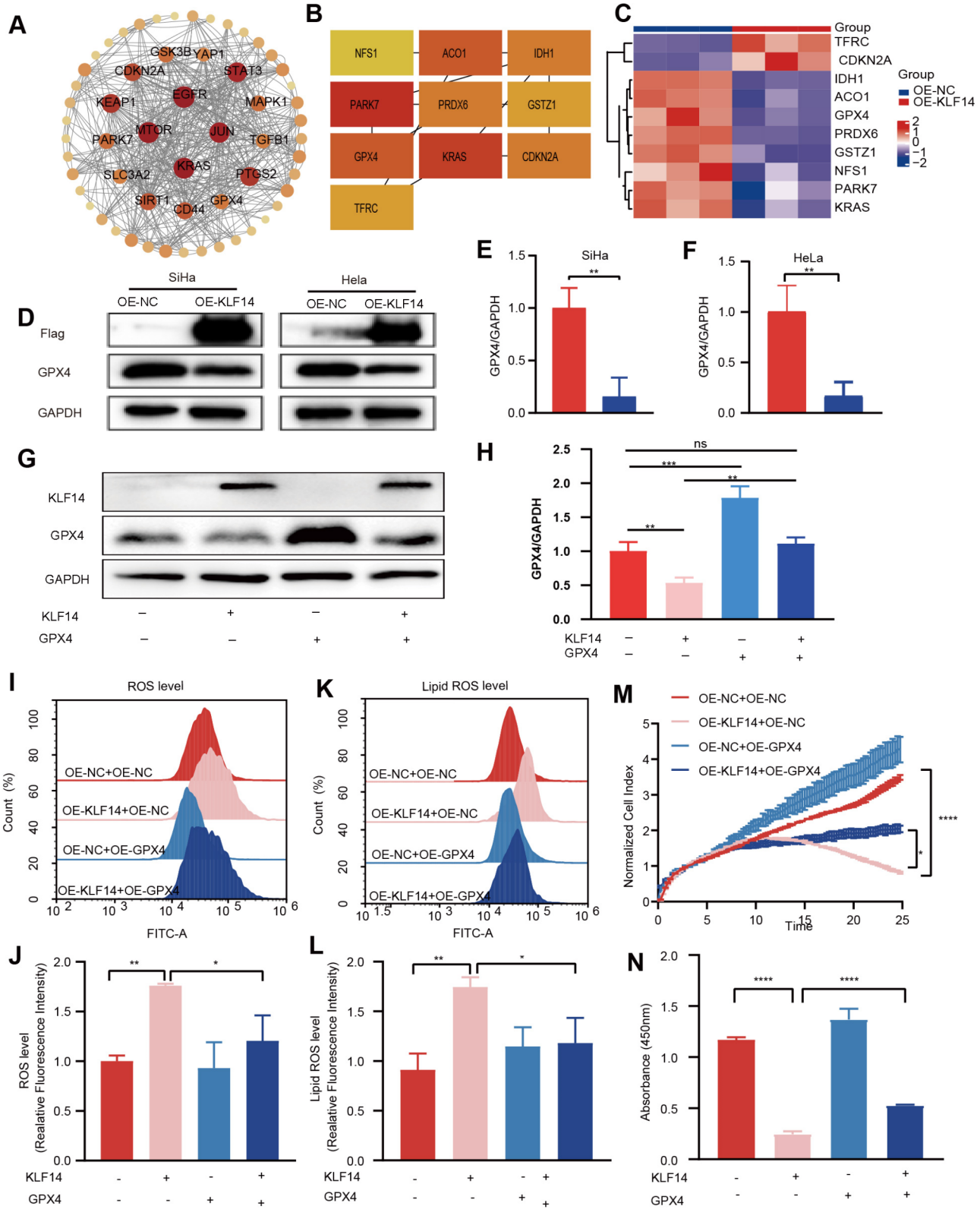

Fig. 5 (See legend on next page.)

(See figure on previous page.)

Fig. 5 KLF14 induces ferroptosis and inhibits cell proliferation by negatively regulating GPX4. (**A**) PPI network analysis of the 66 ferroptosis-related DEGs using STRING and Cytoscape. (**B**) The top ten hub genes were identified by CytoHubba (bottleneck method). The red nodes represent genes with high bottleneck scores, whereas the yellow nodes represent genes with low bottleneck scores. (**C**) Heatmap of the 10 hub genes. (**D**) Immunoblot analysis of GPX4 expression in SiHa and HeLa cells stably expressing KLF14 and the corresponding control cells. *N* = 3 independent repeats. (**E**-**F**) Semiquantitative analysis of GPX4 expression based on WB analysis. The data are presented as the means ± SDs. p values were calculated via an unpaired t test. (**G**) Verification of simultaneous and individual overexpression of KLF14 and GPX4 in SiHa cells via Western blotting. *N* = 3 independent repeats. (**H**) Semiquantitative analysis of GPX4 expression based on WB analysis. The data are presented as the means ± SDs. p values were calculated using one-way ANOVA test. (**I**-**L**) The levels of ROS (**I, J**) and lipid ROS (**K**,**L**) were determined in SiHa cells following simultaneous and individual overexpression of KLF14 and GPX4. The data are presented as the means ± SDs; *N* = 3 independent repeats. p values were calculated via one-way ANOVA test. (**M**-**N**) The effects of GPX4 and KLF14 on cell proliferation were evaluated via RTCA (**M**, each experiment was performed with 2 technical repeats and was independently repeated three times. p values were calculated via the Kruskal-Wallis test) and the CCK-8 assay (**N**, each experiment was performed with 3 technical repeats and was independently repeated three times. The data are presented as the means ± SDs. p values were calculated by one-way ANOVA test). *$p < 0.05$, **$p < 0.01$, ***$p < 0.001$, ****$p < 0.0001$

(as shown in Fig. 6H). Furthermore, CUT&Tag-seq analysis revealed significant enrichment of KLF14 in the *GPX4* gene promoter region (Fig. 7A); The enrichment of KLF14 in the *GPX4* promoter region was nearly 30-fold greater than that in the control group. Compared with that in the control IgG group, the *GPX4* promoter was significantly enriched by KLF14. Therefore, we investigated whether KLF14 directly modulates GPX4 expression via a transcriptional mechanism.

We first analyzed the promoter region of the *GPX4* gene to search for transcription factor-binding sites in the JASPAR database and found that it contains six highly conserved KLF14 binding sites (Fig. 3S A). To further demonstrate that KLF14 represses *GPX4* transcription by binding to its promoter, we constructed a dual-luciferase reporter vector containing the *GPX4* promoter. KLF14 effectively inhibited *GPX4* promoter activity, as demonstrated in Fig. 7B. The result is consistent with the CUT&Tag results mentioned earlier, indicating KLF14 may bind to the promoter of *GPX4* and repress its expression. Next, we performed a promoter truncation analysis to identify the KLF14-responsive region in the *GPX4* promoter. The transcriptional repression of *GPX4* by KLF14 was maintained in cells transfected with the promoter sequence containing −500 to 0 bp (Fig. 7C), indicating the presence of functional binding sites for KLF14 within this truncated promoter region. Three potential binding sites for KLF14 (P1, P2 and P3) were identified in the *GPX4* promoter region (bp −350 bp to +50) (Fig. 3S B). To investigate the KLF14 binding sites, we mutated each site individually or all three sites simultaneously. Luciferase reporter assays revealed that point mutations at specific sites within the *GPX4* promoter did not completely abrogate the inhibitory effect of KLF14 on GPX4. Notably, mutations at sites P1 and P3 attenuated the inhibitory activity of KLF14 on the *GPX4* promoter compared with the wild-type sequence (Fig. 7D). To further verify that KLF14 binds to the promoter region of GPX4, we constructed dual-luciferase reporter gene vectors with sequential deletions of the GPX4 promoter at -500 to 0 bp, -1000 to 0 bp, and −1500 to 0 bp. Following a dual-luciferase reporter gene assay, we observed that the inhibitory effect of KLF14 on GPX4 was disappeared after the deletion of the sequences from −1000 to 0 bp and −1500 to 0 bp (Fig. 7E). These results indicate that KLF14 interacts with several specific sites within the GPX4 promoter region, particularly between −1000 and 0 bp, to exert its suppressive effect.

In humans, the KLF14 gene is intronless, and the KLF14 protein contains 3 Kruppel-like C2H2 zinc fingers at the C-terminal DNA-binding domain. To assess whether the integrity of the three zinc finger domains is essential for KLF14 to exert its transcriptional repression function, we constructed three truncation mutants and transfected them into SiHa cells (Fig. 3S C). Western blot analysis shows no difference in the flag-tagged protein expression levels between the wild-type and the zinc-finger motif mutants of KLF14 (Fig. 7F-G). In contrast, immunofluorescence reveals a notably reduced fluorescence intensity in the mutants, which may be due to the mutation affecting certain characteristics of the protein (Fig. 7H). Next, we performed a dual luciferase reporter assay. Compared with full-length KLF14, the KLF14 binding site truncation mutants Del-1, Del-2 and Del-3 strongly attenuated the repressive effect on the *GPX4*-luciferase reporter (Fig. 7I). RTCA (Fig. 7J) and CCK-8 (Fig. 7K) assays revealed that, compared with the intact structure of KLF14, the deletion of any single zinc finger domain in KLF14 resulted in the loss of its inhibitory effect on the proliferation of SiHa cells. These results showed that the ability of KLF14 to inhibit GPX4 and suppress cell proliferation is dependent on its three zinc finger domains.

KLF14 inhibits GPX4 expression and induces ferroptosis to suppress cervical cancer proliferation in vivo

Next, we tested whether KLF14 overexpression can induce ferroptosis in vivo in a xenograft mouse model. SiHa cells stably expressing KLF14 or control cells generated via a lentiviral expression system were injected subcutaneously into nude mice. Tumor growth in the KLF14-overexpressing group was significantly slower than that in the control group (Fig. 4S A). Moreover, the xenograft tumors were smaller in the nude mice in the

KLF14 overexpression group than in the control group (Fig. 4S B), implying that KLF14 overexpression inhibited tumor cell proliferation in vivo. We next investigated the function of KLF14 in regulating GPX4 in vivo. Tumor tissues were randomly collected and subjected to western blotting and IHC staining to evaluate GPX4 expression. The protein expression level of GPX4 was lower in the KLF14-overexpressing group than in the control group (Fig. 8A-B and D).

To further evaluate whether KLF14 facilitates ferroptosis in cervical cancer xenografts in vivo, we isolated tumor tissues and subsequently performed TEM and IHC staining for 4-HNE, a hallmark of ferroptotic cell death. We found that KLF14 overexpression resulted in smaller mitochondria with fewer cristae (Fig. 8C). As expected, the results of IHC staining of tumor tissues revealed that overexpression of KLF14 led to the suppression of GPX4 expression and an increase in the 4-HNE level, suggesting that KLF14 overexpression may facilitate ferroptosis in vivo (Fig. 8D).

Together, these in vivo results were consistent with those observed in vitro. Therefore, both in vivo and in vitro experiments confirmed that KLF14 can efficiently repress the expression of GPX4 and subsequently increase ferroptosis, thereby inhibiting the proliferation of cervical cancer cells.

Discussion

Most of the current literature on KLF14 emphasizes its critical roles in regulating metabolism, cell proliferation and apoptosis, with its other biological activities remaining largely unexplored. Notably, a recent study revealed that KLF14, primarily by regulating cellular iron metabolism, functions as a tumor suppressor that inhibits the proliferation of hepatocellular carcinoma (HCC) cells [24], suggesting that KLF14 may play other roles in cancer biology. Our study makes three significant contributions. First, we expanded the known biological functions of KLF14 and elucidated a novel molecular pathway through which KLF14 positively regulates ferroptosis in cervical cancer cells. Second, for the first time, we demonstrated that the transcription factor KLF14 can target *GPX4* and regulate its expression by binding to its promoter. Third, we found that a truncation mutation in the zinc finger domain of KLF14 not only significantly reduced its expression levels but also appeared to diminish its repressive function on the *GPX4* promoter. This alteration may be associated with a potential reduction in its tumor suppressive activity in cervical cancer cells. Taken together, these findings suggest that KLF14 might emerge as a promising therapeutic target for the treatment of cervical cancer.

In fact, early work on KLF14 focused mainly on its participation in lipid metabolism and glucose metabolism known as "conducting the metabolic syndrome orchestra" [31–33]. Since KLF14 was first identified as a tumor suppressor gene, its potential role in tumorigenesis has received increasing attention [22, 23, 25]. Programmed cell death generally plays a crucial role in the development and treatment of various cancers. The mechanisms of cell death in cancer cells are particularly complex and potentially involve multiple pathways. In our previous study, we demonstrated that KLF14 significantly promoted apoptosis in cervical cancer cells, thereby inhibiting their proliferation. In this study, LDH assays and dead/live cell staining revealed that overexpression of KLF14 resulted in an increased LDH release and a significant increase in the number of dead cells, suggesting that KLF14 may impair cell membrane integrity and contribute to cell death. Ferroptosis, a newly described form of regulated cell death, is an iron-dependent and lipid peroxidation-driven form of programmed cell death that has been relatively infrequently reported in the context of cervical cancer. Ferroptosis was reported to disrupt the cell membrane's structural integrity [34]. Modulating ferroptosis has emerged as a promising strategy for cancer treatment [35–37]. These findings suggest that KLF14 suppresses cell proliferation not only through apoptosis but also through other pathways, such as ferroptosis. However, to our knowledge, there are currently no reports on the relationship between KLF14 and ferroptosis. Here, we linked KLF14 to roles in regulating both ferroptosis and cervical cancer growth and explored the underlying mechanisms involved.

In the present study, we discovered that the ferroptosis inhibitor lip-1 could partially reverse the suppressed proliferation caused by the overexpression of KLF14. In addition, we found that KLF14 overexpression significantly increased lipid ROS and ROS levels in SiHa and HeLa cells. Consistent with our results, previous reports have indicated that KLF14 transcriptionally activates PLK1, thus inducing the accumulation of ROS [38]. Moreover, the role of KLF14 in enhancing the accumulation of ROS and lipid ROS was comparable to or even exceeded the effects observed with RSL3. Previous reports have suggested that mitochondria are a primary source of ROS in cells, and that several mitochondrial defects trigger the production of ROS [39]. Our electron microscopy results indicated that overexpression of KLF14 leads to destruction of the mitochondrial structure. These findings suggest that KLF14 may disrupt mitochondrial integrity, resulting in increased ROS release into the cytoplasm, or potentially impair the ROS clearance machinery. In addition, an increase in the intracellular Fe^{2+} concentration and alterations in mitochondrial morphology were detected in SiHa cells. In contrast to our observations, the latest research has shown that KLF14 is highly correlated with intracellular iron metabolism, and that KLF14

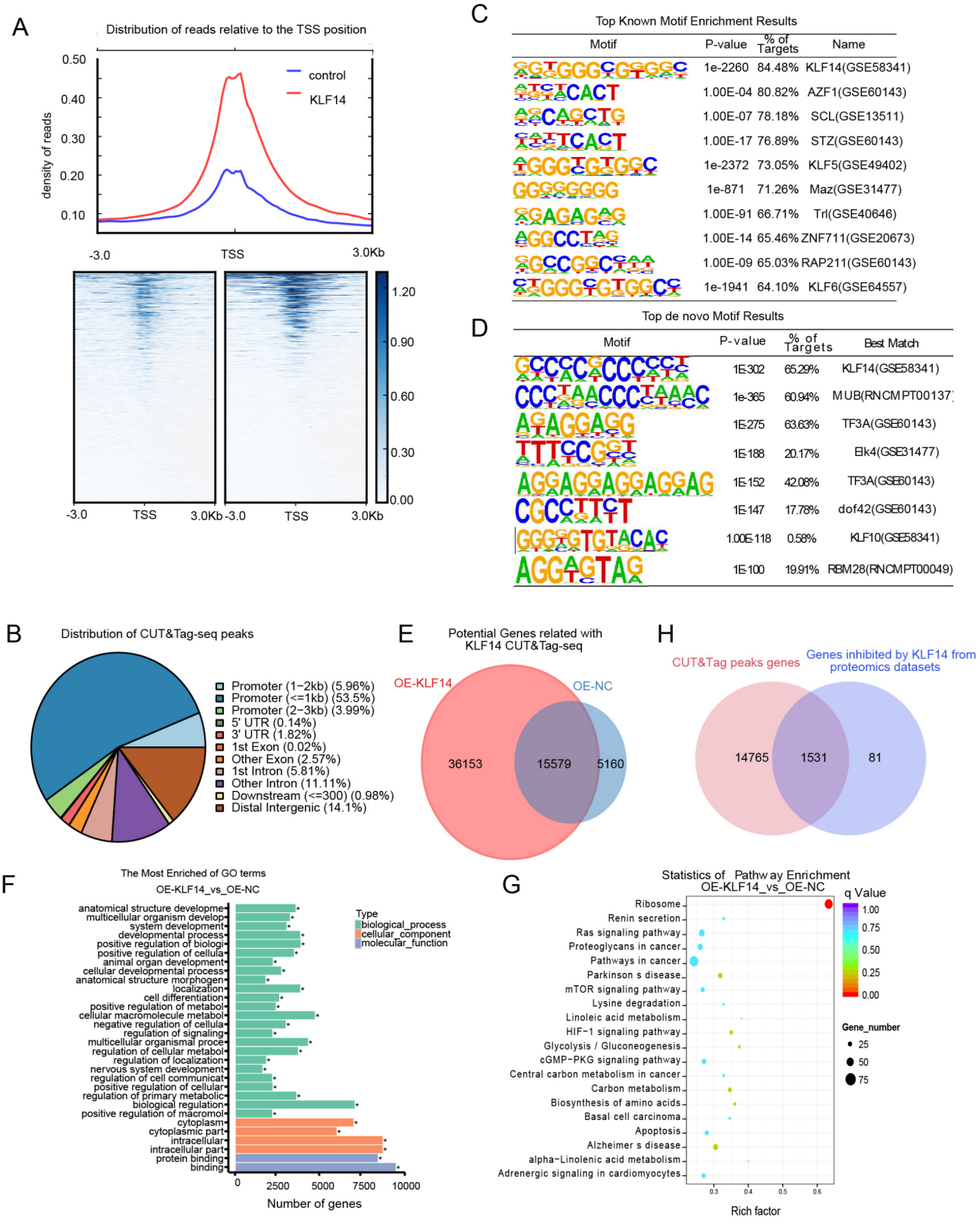

Fig. 6 CUT&Tag analysis of KLF14-overexpressing and control SiHa cells. (**A**) Distribution of KLF14 binding sites relative to the TSS. (**B**) Distribution of KLF14-enriched peaks relative to annotated regions in the genome. (**C**) Known motif enrichment analysis of KLF14 peaks in promoter regions via HOMER. (**D**) De novo motif enrichment analysis of KLF14 peaks in promoter regions via HOMER. (**E**) Overlap analysis of genes containing KLF14 peaks around the TSS with the significantly differentially expressed genes. (**F**-**G**) GO (**F**) and KEGG (**G**) analysis results of genes with significantly differential peaks. (**H**) Overlap analysis of the CUT&Tag-seq data and genes inhibited by KLF14 in proteomic datasets

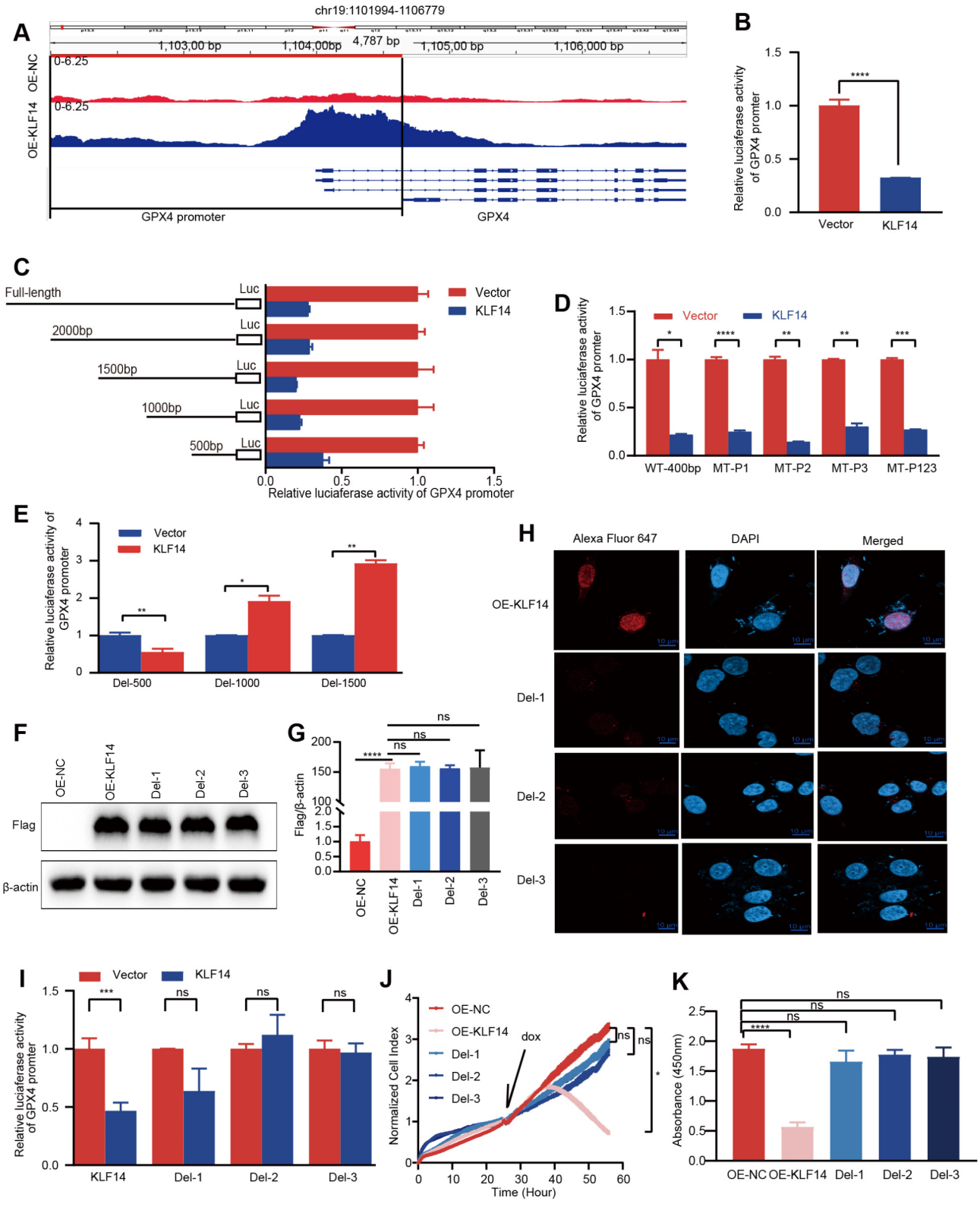

Fig. 7 (See legend on next page.)

(See figure on previous page.)

Fig. 7 KLF14 directly binds to the GPX4 promoter region to inhibit GPX4 transcription. (**A**) Integrative Genomics Viewer (IGV) visualization of the CUT&Tag signals of KLF14 at the GPX4 promoter locus. (**B**) Luciferase reporter assay of GPX4 promoter activity in HEK293 cells with or without KLF14 overexpression. Each experiment was performed with 3 technical repeats and was independently repeated three times. The data are presented as the means ± SDs. p values were calculated by an unpaired t test. (**C**) Promoter truncation assay to locate the KLF14 regulatory region in the GPX4 promoter. (Left) Schematic representation of the truncated GPX4 promoter constructs. (Right) Luciferase values calculated in the reporter assays with the empty vector or KLF14 expression constructs. Each experiment was performed with at least two technical replicates and was independently repeated three times.The data are presented as the means ± SDs. p values were calculated by two-way ANOVA. (**D**) Dual luciferase assay with P1, the P2, P3 and P123 mutants. Each experiment was performed with at least two technical replicates and was independently repeated three times. The data are presented as the means ± SDs. p values were calculated by two-way ANOVA. (**E**) Dual luciferase assay with Del 0–500 bp, 0–1000 bp and 0–1500 bp of *GPX4* promoter. Each experiment was performed with at least two technical replicates and was independently repeated three times. The data are presented as the means ± SDs. p values were calculated by two-way ANOVA. (**F**) Western blotting using an anti-Flag antibody was performed to detect the expression of Flag-tagged wild-type KLF14 and its various zinc-finger motif mutants. $N = 3$ independent repeats. (**G**) Semiquantitative analysis of Flag expression based on WB analysis. The data are presented as the means ± SDs. p values were calculated using one-way ANOVA test. (**H**) Immunofluorescence images of truncated KLF14 proteins in SiHa cells (Red: KLF14; blue: nucleus). The data are presented as the means ± SDs; $N = 3$ repeats. (**I**) Luciferase reporter assay of GPX4 promoter activity in HEK293 cells with the WT-KLF14 and mutated KLF14 constructs. Each experiment was performed with at least two technical replicates and was independently repeated three times. The data are presented as the means ± SDs. p values were calculated by two-way ANOVA.(**J**-**K**) The effects of truncated KLF14 on cell proliferation were evaluated by RTCA (**J**, each experiment was performed with 2 technical repeats and was independently repeated three times. p values were calculated by the Kruskal-Wallis test) and the CCK-8 assay (**K**, each experiment was performed with 3 technical repeats and was independently repeated three times. The data are presented as the means ± SDs. p values were calculated by one-way ANOVA test). *$p < 0.05$, **$p < 0.01$, ***$p < 0.001$, ****$p < 0.0001$

knockdown increases the internal iron concentration in hepatocellular carcinoma cells [24]. This discrepancy may stem from differences in the experimental methodology and cell types used. The authors of the referenced study measured the level of intracellular free iron, whereas we quantified only intracellular Fe^{2+}. Therefore, inducing ferroptosis may be a novel mechanism by which KLF14 inhibits the proliferation of cervical cancer cells.

GPX4, a central regulator of ferroptosis [13], is also an essential regulator of ferroptotic cancer cell death and has been reported to be involved in many pathological processes [40]. Accumulating evidence indicates that transcription factors or cofactors, by binding to the promoter region of *GPX4* and inhibiting or promoting *GPX4* transcription, play a role in regulating ferroptosis, thereby influencing the development and progression of various diseases [41–44]. Recently, GPX4 was linked to therapeutic resistance in cancer and was found to exhibit strong synergistic effects to induce the death of drug-resistant cancer cells, suggesting that targeting *GPX4* may be a strategy for overcoming or preventing acquired drug resistance [45–49].

Here, our results indicated that KLF14 can suppress the expression of GPX4. Moreover, the overexpression of GPX4 partially reversed the increases in the ROS and lipid ROS levels and the inhibition of cell proliferation induced by KLF14 overexpression. We speculated that KLF14 triggered ferroptosis possibly by suppressing GPX4 expression, thereby inhibiting cervical cancer cell proliferation. This finding was further confirmed by a dual luciferase reporter assay. We found for the first time that overexpressing KLF14 downregulated the expression and activity of *GPX4* by directly binding to the *GPX4* promoter region. These results may explain why KLF14 had additive or synergistic promoting effects with RSL3 in increasing the levels of ROS and lipid ROS in cervical cancer cells. RSL3 is identified as a potent ferroptosis activator that binds directly to and inhibits the activity of GPX4 [13], leading to a rapid accumulation of lipid ROS and ferroptosis. It is likely due to their combined targeting of GPX4. KLF14 inhibits the transcription of *GPX4*, whereas RSL3 inhibits the enzymatic activity of GPX4. The dual inhibition effect results in a significant reduction in both the quantity and functionality of GPX4. The combined effects of KLF14 and RSL3 on GPX4 offer a novel avenue for therapeutic intervention, which specifically targets conditions that benefit from the induction of ferroptosis. Although the introduced mutations in the binding sites of KLF14 in the *GPX4* promoter region did not completely abolish the inhibition of *GPX4* transcription, our studies have confirmed that KLF14 indeed binds within the region of *GPX4* promoter from −1000 to the TSS. The current study provides evidence that KLF14 may suppress GPX4 expression through interactions with multiple sites within the promoter region and implies the potential involvement of additional unidentified binding sites or mechanisms in the repression of GPX4 by KLF14. Furthermore, the differential impacts of various sites on the repressive activity of KLF14 indicate their distinct roles in the transcriptional repression mediated by KLF14. This finding suggests that modulating these sites could be a therapeutic strategy for conditions sensitive to GPX4 levels. Therefore, our data further imply that KLF14, which inhibits tumor growth in cervical cancer through targeted inhibition of GPX4, is a potential target for cancer treatment.

Within the KLF family, KLF14 is the only gene without introns. It possesses three DNA-binding zinc finger domains through which it regulates the transcription of various genes. Previous studies have shown that the KLF14-M4 mutant, with a mutation of four amino acids to alanine, exhibited a significantly reduced inhibitory

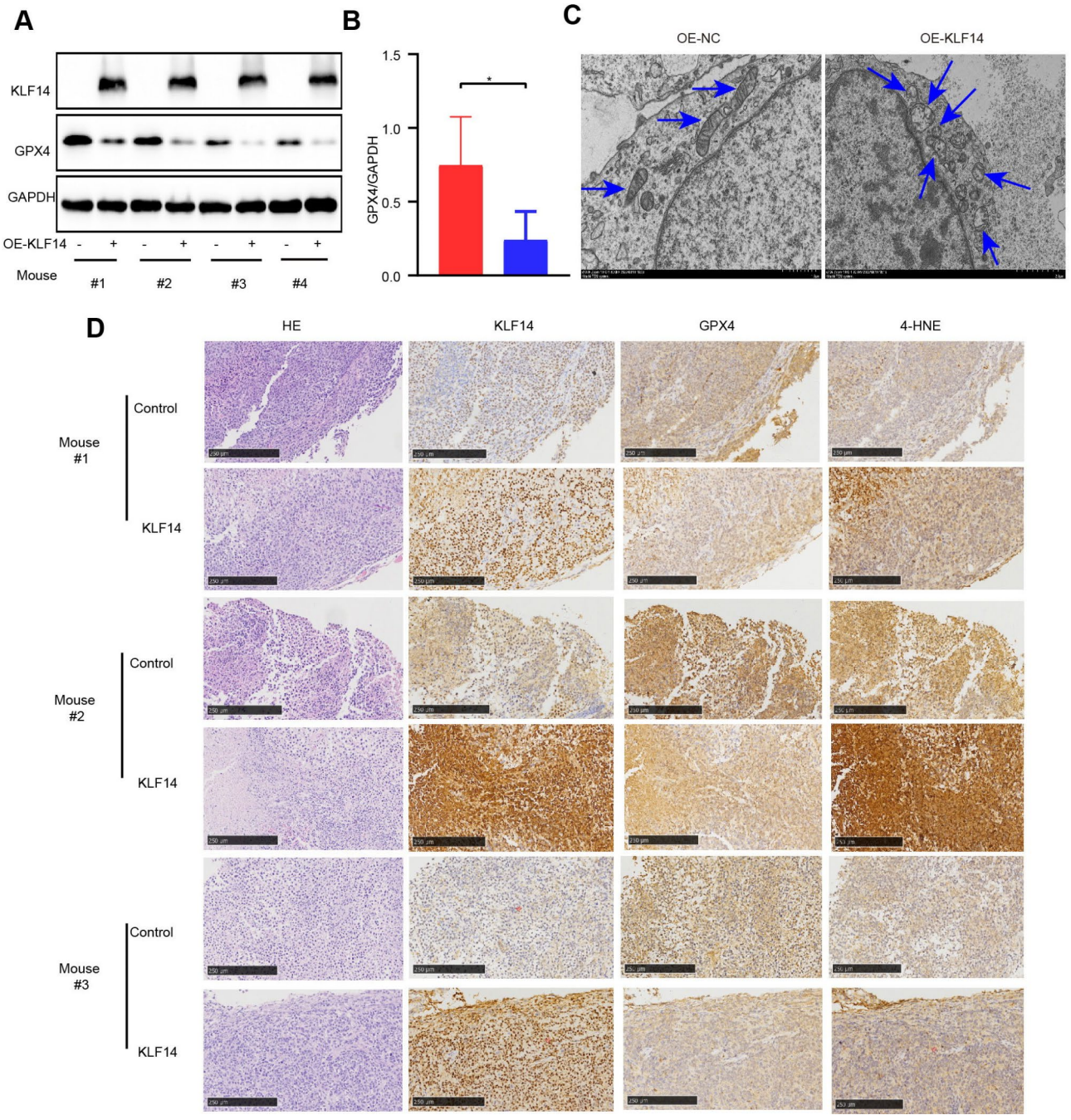

Fig. 8 KLF14 inhibits GPX4 expression and induces ferroptosis to suppress cervical cancer cell proliferation in vivo. (**A**) WB analysis of KLF14 and GPX4 expression in representative tumors. The data are presented as the means ± SDs; $n = 3$ repeats. (**B**) Semiquantitative analysis of GPX4 expression based on WB analysis. The data are presented as the means ± SDs. p values were calculated using an unpaired t test. (**C**) Electron microscopy analysis of xenograft tumors (blue arrows represent mitochondria). (**D**) HE staining and immunohistochemical staining (for KLF14, 4-HNE and GPX4) of Siha xenograft tumors. *$p < 0.05$

effect on IRP2 promoter activity [24]. Here, we observed that the KLF14 zinc finger truncation mutation resulted in the loss of the ability to repress *GPX4* promoter activity, likely because the absence of the zinc finger binding site prevents KLF14 from binding to the DNA-binding domain in the *GPX4* promoter. Additionally, in parallel with the observed decrease in *GPX4* promoter repression, the KLF14 zinc finger truncation mutation also resulted in the loss of its inhibitory effect on SiHa cell proliferation. These findings suggest that the intact zinc finger domain of KLF14 is crucial not only crucial for its interaction with the *GPX4* promoter but also for

executing its tumor suppressive function in cervical cancer cells. The absence of the zinc finger binding site likely disrupts KLF14's DNA-binding ability, thereby attenuating its regulatory effects on GPX4 and its subsequent impact on cell proliferation.

Conclusions

In summary, these new mechanistic findings reveal the role of KLF14 in the regulation of ferroptosis in cervical cancer and identify novel approaches for the development of anticancer therapeutics and strategies.

Abbreviations

IHC	Immunohistochemistry
CCK-8	Cell Counting Kit-8
RTCA	Real-time Cell Analysis
TEM	Transmission Electron Microscopy
HPV	Human Papillomavirus
GSH	Glutathione
lncRNA	Long Noncoding RNA
ROS	Reactive Oxygen Species
CTCC	Chinese Tissue Culture Collection
ATCC	American Type Culture Collection
DMEM	Dulbecco's Modified Eagle Medium
FBS	Fetal Bovine Serum
HE	Hematoxylin/Eosin
RIPA	Radioimmunoprecipitation Assay
ECL	Enhanced Chemiluminescence
DOX	Doxycycline
TSS	Transcription Start Sites
IGV	Integrative Genomics Viewer
TCGA	The Cancer Genome Atlas
HPA	Human Protein Atlas
TMT	Tandem Mass Tag
KEGG	Kyoto Encyclopedia of Genes and Genomes
STRING	Search Tool for the Retrieval of Interacting Genes/Proteins
HOMER	Hypergeometric Optimization of Motif Enrichment
4-HNE	4-Hydroxynonenal
HCC	Hepatocellular Carcinoma
DEPs	Expressed Proteins
Lip-1	Liproxstatin-1
OS	Overall Survival
RFS	Relapse Free Survival
BRCA	Breast invasive Carcinoma
KICH	Kidney Chromophobe
KIRP	Kidney Renal Papillary Cell Carcinoma
LUSC	Lung Squamous Cell Carcinoma
PCPG	Pheochromocytoma and Paraganglioma
STAD	Stomach Adenocarcinoma
UCEC	Uterine Corpus Endometrial Carcinoma
ESCA	Esophageal Carcinoma
BLCA	Bladder Urothelial Carcinoma
CHOL	Cholangiocarcinoma
HNSC	Head and Neck Squamous Cell Carcinoma
LIHC	Liver Hepatocellular Carcinoma
THCA	Thyroid Carcinoma
LUAD	Lung Adenocarcinoma
TGCT	Testicular Germ Cell Tumor

Supplementary Information

The online version contains supplementary material available at https://doi.org/10.1186/s12967-024-05714-6.

Supplementary Material 1: Figure 1S: KLF14 is expressed at low levels in cervical cancer patients. (A) Immunohistochemical analysis of KLF14 expression in cervical cancer tissues and adjacent tissues in a tissue microarray (n?=?31). (B) KLF14 expression scores in these tissues were calculated as the product of the staining intensity and positive rate (score = staining intensity x positive rate). (C-E) KLF14 overexpression was confirmed by Western blotting in SiHa and HeLa cells. All the cell experiments were independently repeated for three times. The data are shown as the means±SDs. A paired t-test was used to compare two groups. *p<0.05, ****p<0.0001.

Supplementary Material 2: TMT-based quantitative proteomics, proteome sequencing and data analysis in SiHa cells overexpressing KLF14. (A) Heatmap of DEPs. (B-C) GO enrichment analysis of the DEPs. (D) The top 20 KEGG pathways enriched with the DEPs are shown in a bubble chart. (E) Protein?protein interaction (PPI) network of the significant DEPs.

Supplementary Material 3: Schematic illustration. (A) Schematic diagram of binding sites predicted via the JASPAR database. (B) Schematic illustration of KLF14 binding sites in the promoter region of GPX4 (-350-+50) and site-directed mutagenesis. (C) Schematic representation of the full-length and truncated constructs of human KLF14.

Supplementary Material 4: KLF14 inhibits cervical cancer in vivo. (A) The growth curves of tumor volumes; n = 6. (p values were calculated by two-way ANOVA test) (B): Representative image of xenograft tumors (n = 6).

Supplementary Material 5: The DEGs list: expression profiles of 66 ferroptosis genes following KLF14 overexpression.

Acknowledgements

Thanks to the public databases for providing us with data.

Author contributions

Conceptualization, L.C., H.Y.; Investigation, H.Y., X.D., X.L., Y.D., J.Q.; Data Curation, R.G.; Formal Analysis, H.Y., R.G.; Supervision, L.C.; Writing - Original Draft, H.Y.; Writing - Review & Editing, L.C.; Visualization, H.Y., R.G.; Project Administration, L.C.; Funding Acquisition, L.C.

Funding

This work was supported by the Shandong Provincial Natural Science Foundation (ZR2020MH203).

Data availability

The study's original contributions are detailed in the article. Further inquiries can be directed to the corresponding authors.

Declarations

Ethics approval and consent to participate

The Ethics Committee of the First Affiliated Hospital of Shandong First Medical University approved this experiment (SYDWLS2020016).

Consent for publication

All authors consented for publication.

Competing interests

There are no competing interests.

Author details

[1]Oncology Department, Shandong Provincial Qianfoshan Hospital, Shandong University, Jinan 250014, China
[2]Oncology Department, The First Affiliated Hospital of Shandong First Medical University & Shandong Provincial Qianfoshan Hospital, Jinan 250014, China
[3]Shandong Provincial Key Laboratory for Rheumatic Disease and Translational Medicine, Laboratory of Clinical Immunology and Translational Medicine, Shandong Provincial University, Jinan 250014, China
[4]Shandong Lung Cancer Institute, Jinan 250014, China
[5]Blood Center of Shandong Province, Jinan 250014, China
[6]Department of Blood Transfusion, Binzhou People's Hospital, Binzhou 256601, China
[7]Shandong Public Health Clinical Center, Shandong University, Shandong 250013, China

[8]Department of Laboratory Medicine, Linyi Peoples' Hospital, Linyi 276003, China
[9]Department of Clinical Laboratory Medicine, The First Affiliated Hospital of Shandong First Medical University & Shandong Provincial Qianfoshan Hospital, Jinan 250014, China

Received: 5 June 2024 / Accepted: 30 September 2024
Published online: 10 October 2024

References

1. Castle PE, Einstein MH, Sahasrabuddhe VV. Cervical cancer prevention and control in women living with human immunodeficiency virus. CA Cancer J Clin. 2021;71:505–26. https://doi.org/10.3322/caac.21696.
2. Rodin D, Burger EA, Atun R, Barton M, Gospodarowicz M, Grover S, Hanna TP, Jaffray DA, Knaul FM, Lievens Y, Zubizarreta E, Milosevic M. Scale-up of radiotherapy for cervical cancer in the era of human papillomavirus vaccination in low-income and middle-income countries: a model-based analysis of need and economic impact. Lancet Oncol. 2019;20:915–23. https://doi.org/10.1016/S1470-2045(19)30308-0.
3. He C, Lv X, Huang C, Angeletti PC, Hua G, Dong J, Zhou J, Wang Z, Ma B, Chen X, Lambert PF, Rueda BR, Davis JS, Wang C. A human papillomavirus-independent cervical Cancer Animal Model reveals unconventional mechanisms of cervical carcinogenesis. Cell Rep. 2019;26:2636–e26502635. https://doi.org/10.1016/j.celrep.2019.02.004.
4. Dixon SJ, Lemberg KM, Lamprecht MR, Skouta R, Zaitsev EM, Gleason CE, Patel DN, Bauer AJ, Cantley AM, Yang WS, Morrison B. 3rd, Stockwell BR: ferroptosis: an iron-dependent form of nonapoptotic cell death. Cell. 2012;149:1060–72. https://doi.org/10.1016/j.cell.2012.03.042.
5. Verma N, Vinik Y, Saroha A, Nair NU, Ruppin E, Mills G, Karn T, Dubey V, Khera L, Raj H, Maina F, Lev S. Synthetic lethal combination targeting BET uncovered intrinsic susceptibility of TNBC to ferroptosis. Sci Adv. 2020;6. https://doi.org/10.1126/sciadv.aba8968.
6. Zhang Y, Shi J, Liu X, Feng L, Gong Z, Koppula P, Sirohi K, Li X, Wei Y, Lee H, Zhuang L, Chen G, Xiao ZD, Hung MC, Chen J, Huang P, Li W, Gan B. BAP1 links metabolic regulation of ferroptosis to tumour suppression. Nat Cell Biol. 2018;20:1181–92. https://doi.org/10.1038/s41556-018-0178-0.
7. Jiang L, Kon N, Li T, Wang SJ, Su T, Hibshoosh H, Baer R, Gu W. Ferroptosis as a p53-mediated activity during tumour suppression. Nature. 2015;520:57–62. https://doi.org/10.1038/nature14344.
8. Wang C, Zeng J, Li LJ, Xue M, He SL. Cdc25A inhibits autophagy-mediated ferroptosis by upregulating ErbB2 through PKM2 dephosphorylation in cervical cancer cells. Cell Death Dis. 2021;12:1055. https://doi.org/10.1038/s41419-021-04342-y.
9. Wang X, Ji Y, Qi J, Zhou S, Wan S, Fan C, Gu Z, An P, Luo Y, Luo J. Mitochondrial carrier 1 (MTCH1) governs ferroptosis by triggering the FoxO1-GPX4 axis-mediated retrograde signaling in cervical cancer cells. Cell Death Dis. 2023;14:508. https://doi.org/10.1038/s41419-023-06033-2.
10. Gong Y, Luo G, Zhang S, Chen Y, Hu Y. Transcriptome sequencing analysis reveals miR-30c-5p promotes ferroptosis in cervical cancer and inhibits growth and metastasis of cervical cancer xenografts by targeting the METTL3/KRAS axis. Cell Signal. 2024;117:111068. https://doi.org/10.1016/j.cellsig.2024.111068.
11. Wang M, Mao C, Ouyang L, Liu Y, Lai W, Liu N, Shi Y, Chen L, Xiao D, Yu F, Wang X, Zhou H, Cao Y, Liu S, Yan Q, Tao Y, Zhang B. Long noncoding RNA LINC00336 inhibits ferroptosis in lung cancer by functioning as a competing endogenous RNA. Cell Death Differ. 2019;26:2329–43. https://doi.org/10.1038/s41418-019-0304-y.
12. Wang J, Yin X, He W, Xue W, Zhang J, Huang Y. SUV39H1 deficiency suppresses clear cell renal cell carcinoma growth by inducing ferroptosis. Acta Pharm Sin B. 2021;11:406–19. https://doi.org/10.1016/j.apsb.2020.09.015.
13. Yang WS, SriRamaratnam R, Welsch ME, Shimada K, Skouta R, Viswanathan VS, Cheah JH, Clemons PA, Shamji AF, Clish CB, Brown LM, Girotti AW, Cornish VW, Schreiber SL, Stockwell BR. Regulation of ferroptotic cancer cell death by GPX4. Cell. 2014;156:317–31. https://doi.org/10.1016/j.cell.2013.12.010.
14. Chen H, Peng F, Xu J, Wang G, Zhao Y. Increased expression of GPX4 promotes the tumorigenesis of thyroid cancer by inhibiting ferroptosis and predicts poor clinical outcomes. Aging. 2023;15:230–45. https://doi.org/10.18632/aging.204473.
15. Wei S, Yu Z, Shi R, An L, Zhang Q, Zhang Q, Zhang T, Zhang J, Wang H. GPX4 suppresses ferroptosis to promote malignant progression of endometrial carcinoma via transcriptional activation by ELK1. BMC Cancer. 2022;22:881. https://doi.org/10.1186/s12885-022-09986-3.
16. Liu Y, Li L, Yang Z, Wen D, Hu Z. Circular RNA circACAP2 suppresses ferroptosis of cervical Cancer during malignant progression by miR-193a-5p/GPX4. J Oncol. 2022;2022(5228874). https://doi.org/10.1155/2022/5228874.
17. Zhang Z, Hu Q, Ye S, Xiang L. Inhibition of the PIN1-NRF2/GPX4 axis imparts sensitivity to cisplatin in cervical cancer cells. Acta Biochim Biophys Sin (Shanghai). 2022;54:1325–35. https://doi.org/10.3724/abbs.2022109.
18. Chen X, Shi W, Zhang H. The role of KLF14 in multiple disease processes. BioFactors. 2020;46:276–82. https://doi.org/10.1002/biof.1612.
19. Fan G, Sun L, Shan P, Zhang X, Huan J, Zhang X, Li D, Wang T, Wei T, Zhang X, Gu X, Yao L, Xuan Y, Hou Z, Cui Y, Cao L, Li X, Zhang S, Wang C. Loss of KLF14 triggers centrosome amplification and tumorigenesis. Nat Commun. 2015;6:8450. https://doi.org/10.1038/ncomms9450.
20. Wu G, Yuan S, Chen Z, Chen G, Fan Q, Dong H, Ye F, Li J, Zhu X. The KLF14 transcription factor regulates glycolysis by Downregulating LDHB in Colorectal Cancer. Int J Biol Sci. 2019;15:628–35. https://doi.org/10.7150/ijbs.30652.
21. Zhou J, Lin J, Zhang H, Zhu F, Xie R. LncRNA HAND2-AS1 sponging miR-1275 suppresses colorectal cancer progression by upregulating KLF14. Biochem Biophys Res Commun. 2018;503:1848–53. https://doi.org/10.1016/j.bbrc.2018.07.125.
22. Chen XZ, He WX, Luo RG, Xia GJ, Zhong JX, Chen QJ, Huang YY, Guan YX. KLF14/miR-1283/TFAP2C axis inhibits HER2-positive breast cancer progression via declining tumor cell proliferation. Mol Carcinog. 2023;62:532–45. https://doi.org/10.1002/mc.23505.
23. Chu J, Hu XC, Li CC, Li TY, Fan HW, Jiang GQ. KLF14 alleviated breast cancer invasion and M2 macrophages polarization through modulating SOCS3/RhoA/Rock/STAT3 signaling. Cell Signal. 2022;92:110242. https://doi.org/10.1016/j.cellsig.2022.110242.
24. Zhou H, Chen J, Fan M, Cai H, Dong Y, Qiu Y, Zhuang Q, Lei Z, Li M, Ding X, Yan P, Lin A, Zheng S, Yan Q. KLF14 regulates the growth of hepatocellular carcinoma cells via its modulation of iron homeostasis through the repression of iron-responsive element-binding protein 2. J Exp Clin Cancer Res. 2023;42:5. https://doi.org/10.1186/s13046-022-02562-4.
25. Wang YG, Liu J, Shi M, Chen FX. LncRNA DGCR5 represses the development of hepatocellular carcinoma by targeting the miR-346/KLF14 axis. J Cell Physiol. 2018;234:572–80. https://doi.org/10.1002/jcp.26779.
26. Lyu X, Ding X, Ye H, Guo R, Wu M, Cao L. KLF14 targets ITGB1 to inhibit the progression of cervical cancer via the PI3K/AKT signalling pathway. Discov Oncol. 2022;13:30. https://doi.org/10.1007/s12672-022-00494-1.
27. Luo XH, Liu JZ, Wang B, Men QL, Ju YQ, Yin FY, Zheng C, Li W. KLF14 potentiates oxidative adaptation via modulating HO-1 signaling in castrate-resistant prostate cancer. Endocr Relat Cancer. 2019;26:181–95. https://doi.org/10.1530/ERC-18-0383.
28. Boot A, Oosting J, de Miranda NF, Zhang Y, Corver WE, van de Water B, Morreau H, van Wezel T. Imprinted survival genes preclude loss of heterozygosity of chromosome 7 in cancer cells. J Pathol. 2016;240:72–83. https://doi.org/10.1002/path.4756.
29. Chandrashekar DS, Bashel B, Balasubramanya SAH, Creighton CJ, Ponce-Rodriguez I, Chakravarthi B, Varambally S. UALCAN: a portal for facilitating Tumor Subgroup Gene expression and survival analyses. Neoplasia. 2017;19:649–58. https://doi.org/10.1016/j.neo.2017.05.002.
30. Gyorffy B. Integrated analysis of public datasets for the discovery and validation of survival-associated genes in solid tumors. Innov (Camb). 2024;5:100625. https://doi.org/10.1016/j.xinn.2024.100625.
31. Small KS, Hedman AK, Grundberg E, Nica AC, Thorleifsson G, Kong A, Thorsteindottir U, Shin SY, Richards HB, Consortium G, Investigators M, Consortium D, Soranzo N, Ahmadi KR, Lindgren CM, Stefansson K, Dermitzakis ET, Deloukas P, Spector TD, McCarthy MI, Mu TC. Identification of an imprinted master trans regulator at the KLF14 locus related to multiple metabolic phenotypes. Nat Genet. 2011;43:561–4. https://doi.org/10.1038/ng.833.
32. Civelek M, Lusis AJ. Conducting the metabolic syndrome orchestra. Nat Genet. 2011;43:506–8. https://doi.org/10.1038/ng.842.
33. de Assuncao TM, Lomberk G, Cao S, Yaqoob U, Mathison A, Simonetto DA, Huebert RC, Urrutia RA, Shah VH. New role for Kruppel-like factor 14 as a transcriptional activator involved in the generation of signaling lipids. J Biol Chem. 2014;289:15798–809. https://doi.org/10.1074/jbc.M113.544346.
34. Yan B, Ai Y, Sun Q, Ma Y, Cao Y, Wang J, Zhang Z, Wang X. Membrane damage during ferroptosis is caused by oxidation of phospholipids catalyzed by the oxidoreductases POR and CYB5R1. Mol Cell. 2021;81:355–e369310. https://doi.org/10.1016/j.molcel.2020.11.024.

35. Lei G, Zhang Y, Koppula P, Liu X, Zhang J, Lin SH, Ajani JA, Xiao Q, Liao Z, Wang H, Gan B. The role of ferroptosis in ionizing radiation-induced cell death and tumor suppression. Cell Res. 2020;30:146–62. https://doi.org/10.1038/s41422-019-0263-3.
36. Wang W, Green M, Choi JE, Gijon M, Kennedy PD, Johnson JK, Liao P, Lang X, Kryczek I, Sell A, Xia H, Zhou J, Li G, Li J, Li W, Wei S, Vatan L, Zhang H, Szeliga W, Gu W, Liu R, Lawrence TS, Lamb C, Tanno Y, Cieslik M, Stone E, Georgiou G, Chan TA, Chinnaiyan A, Zou W. CD8(+) T cells regulate tumour ferroptosis during cancer immunotherapy. Nature. 2019;569:270–4. https://doi.org/10.1038/s41586-019-1170-y.
37. Lei G, Zhuang L, Gan B. Targeting ferroptosis as a vulnerability in cancer. Nat Rev Cancer. 2022;22:381–96. https://doi.org/10.1038/s41568-022-00459-0.
38. Hao JS, Zhu CJ, Yan BY, Yan CY, Ling R. Stimulation of KLF14/PLK1 pathway by thrombin signaling potentiates endothelial dysfunction in type 2 diabetes mellitus. Biomed Pharmacother. 2018;99:859–66. https://doi.org/10.1016/j.biopha.2018.01.151.
39. Sarmiento-Salinas FL, Perez-Gonzalez A, Acosta-Casique A, Ix-Ballote A, Diaz A, Trevino S, Rosas-Murrieta NH, Millan-Perez-Pena L, Maycotte P. Reactive oxygen species: role in carcinogenesis, cancer cell signaling and tumor progression. Life Sci. 2021;284:119942. https://doi.org/10.1016/j.lfs.2021.119942.
40. Stockwell BR, Jiang X, Gu W. Emerging mechanisms and Disease Relevance of Ferroptosis. Trends Cell Biol. 2020;30:478–90. https://doi.org/10.1016/j.tcb.2020.02.009.
41. Wang Y, Yan S, Liu X, Deng F, Wang P, Yang L, Hu L, Huang K, He J. PRMT4 promotes ferroptosis to aggravate doxorubicin-induced cardiomyopathy via inhibition of the Nrf2/GPX4 pathway. Cell Death Differ. 2022;29:1982–95. https://doi.org/10.1038/s41418-022-00990-5.
42. Wang Y, Zheng L, Shang W, Yang Z, Li T, Liu F, Shao W, Lv L, Chai L, Qu L, Xu Q, Du J, Liang X, Zeng J, Jia J. Wnt/beta-catenin signaling confers ferroptosis resistance by targeting GPX4 in gastric cancer. Cell Death Differ. 2022;29:2190–202. https://doi.org/10.1038/s41418-022-01008-w.
43. Han X, Duan X, Liu Z, Long Y, Liu C, Zhou J, Li N, Qin J, Wang Y. ZEB1 directly inhibits GPX4 transcription contributing to ROS accumulation in breast cancer cells. Breast Cancer Res Treat. 2021;188:329–42. https://doi.org/10.1007/s10549-021-06301-9.
44. Wang Z, Zhang X, Tian X, Yang Y, Ma L, Wang J, Yu Y. CREB stimulates GPX4 transcription to inhibit ferroptosis in lung adenocarcinoma. Oncol Rep. 2021;45. https://doi.org/10.3892/or.2021.8039.
45. Hangauer MJ, Viswanathan VS, Ryan MJ, Bole D, Eaton JK, Matov A, Galeas J, Dhruv HD, Berens ME, Schreiber SL, McCormick F, McManus MT. Drug-tolerant persister cancer cells are vulnerable to GPX4 inhibition. Nature. 2017;551:247–50. https://doi.org/10.1038/nature24297.
46. Koenders STA, Wijaya LS, Erkelens MN, Bakker AT, van der Noord VE, van Rooden EJ, Burggraaff L, Putter PC, Botter E, Wals K, van den Elst H, den Dulk H, Florea BI, van de Water B, van Westen GJP, Mebius RE, Overkleeft HS, Le Devedec SE, van der Stelt M. Development of a retinal-based probe for the profiling of Retinaldehyde dehydrogenases in Cancer cells. ACS Cent Sci. 2019;5:1965–74. https://doi.org/10.1021/acscentsci.9b01022.
47. Viswanathan VS, Ryan MJ, Dhruv HD, Gill S, Eichhoff OM, Seashore-Ludlow B, Kaffenberger SD, Eaton JK, Shimada K, Aguirre AJ, Viswanathan SR, Chattopadhyay S, Tamayo P, Yang WS, Rees MG, Chen S, Boskovic ZV, Javaid S, Huang C, Wu X, Tseng YY, Roider EM, Gao D, Cleary JM, Wolpin BM, Mesirov JP, Haber DA, Engelman JA, Boehm JS, Kotz JD, Hon CS, Chen Y, Hahn WC, Levesque MP, Doench JG, Berens ME, Shamji AF, Clemons PA, Stockwell BR, Schreiber SL. Dependency of a therapy-resistant state of cancer cells on a lipid peroxidase pathway. Nature. 2017;547:453–7. https://doi.org/10.1038/nature23007.
48. Chen Y, Li L, Lan J, Cui Y, Rao X, Zhao J, Xing T, Ju G, Song G, Lou J, Liang J. CRISPR screens uncover protective effect of PSTK as a regulator of chemotherapy-induced ferroptosis in hepatocellular carcinoma. Mol Cancer. 2022;21:11. https://doi.org/10.1186/s12943-021-01466-9.
49. Yang S, Wong KH, Hua P, He C, Yu H, Shao D, Shi Z, Chen M. ROS-responsive fluorinated polyethyleneimine vector to co-deliver shMTHFD2 and shGPX4 plasmids induces ferroptosis and apoptosis for cancer therapy. Acta Biomater. 2022;140:492–505. https://doi.org/10.1016/j.actbio.2021.11.042.

Publisher's note